Research Paper

GEOSPHERE

GEOSPHERE, v. 16, no. 2

https://doi.org/10.1130/GES02168.1

14 figures; 1 plate; 1 set of supplemental files

CORRESPONDENCE: russell.difiori@wsu.edu

CITATION: Di Fiori, R.V., Long, S.P., Fetrow, A.C., Snell, K.E., Bonde, J.W., and Vervoort, J., 2020, Syncontractional deposition of the Cretaceous Newark Canyon Formation, Diamond Mountains, Nevada: Implications for strain partitioning within the U.S. Cordillera: Geosphere, v. 16, no. 2, p. 546–566, https://doi.org/10.1130/GES02168.1.

Science Editor: Andrea Hampel
Associate Editor: Gregory D. Hoke

Received 14 June 2019
Revision received 13 September 2019
Accepted 13 December 2019

Published online 6 January 2020

Syncontractional deposition of the Cretaceous Newark Canyon Formation, Diamond Mountains, Nevada: Implications for strain partitioning within the U.S. Cordillera

Russell V. Di Fiori[1], Sean P. Long[1], Anne C. Fetrow[2], Kathryn E. Snell[2], Joshua W. Bonde[3], and Jeff Vervoort[1]

[1]School of the Environment, P.O. Box 642812, Washington State University, Pullman, Washington 99164, USA
[2]Department of Geological Sciences, University of Colorado–Boulder, Boulder, Colorado 80309, USA
[3]Las Vegas Natural History Museum, 900 Las Vegas Blvd. N., Las Vegas, Nevada 89101, USA

ABSTRACT

The timing of deformation and deposition within syntectonic basins provides critical information for understanding the evolution of strain in mountain belts. In the U.S. Cordillera, contractional deformation was partitioned between the Sevier thrust belt in Utah and several structural provinces in the hinterland in Nevada. One hinterland province, the Central Nevada thrust belt (CNTB), accommodated up to ~15 km of shortening; however, in most places, this deformation can only be bracketed between Permian and Eocene. Cretaceous deposits of the Newark Canyon Formation (NCF), which are sparsely exposed along the length of the CNTB, offer the opportunity to constrain deformation timing. Here, we present mapping and U-Pb zircon geochronology from the NCF in the Diamond Mountains, which demonstrate deposition of the NCF during proximal CNTB deformation. Deposition of the basal NCF member was under way no earlier than ca. 114 Ma, a tuff in the middle part of the section was deposited at ca. 103 Ma, and the youngest member was deposited no earlier than ca. 99 Ma. Intraformational angular unconformities and abrupt along- and across-strike thickness changes indicate that NCF deposition was related to growth of an east-vergent fault-propagation fold. Clast compositions define unroofing of upper Paleozoic sedimentary rocks, which we interpret as the progressive erosion of an anticline ~10 km to the west. CNTB deformation was contemporaneous with shortening in the Sevier thrust belt, which defines middle Cretaceous strain partitioning between frontal and interior components of the Cordillera. Strain partitioning may have been promoted by renewed underthrusting during a period of high-flux magmatism.

INTRODUCTION

Documenting the space-time distribution of contractional deformation is fundamental to understanding how orogenic systems evolve. However, orogenic wedges are dynamic, and often record a complex interplay between deformation at the frontal wedge tip and out-of-sequence thrusting and folding in the internal part of the wedge (e.g., Morley, 1988; Taylor et al., 2000; McQuarrie, 2002; Wells et al., 2012; Long et al., 2014; Anderson et al., 2018). For this reason, analyzing the geometry, timing, and magnitude of deformation within both the frontal and interior portions of an orogenic wedge is crucial for understanding fold-thrust dynamics.

The North American Cordilleran orogen was constructed between the Jurassic and Paleogene (ca. 150–50 Ma) in response to eastward subduction of the Farallon plate beneath North America (e.g., Armstrong, 1968; Allmendinger, 1992; DeCelles, 2004; Dickinson, 2006; Yonkee and Weil, 2015). In the western U.S. portion of the Cordillera, contractional deformation affected a broad retroarc region across Nevada and western Utah (Fig. 1). The majority of shortening (~150–220 km) was accommodated in the Sevier thrust belt in western Utah (e.g., Armstrong, 1968; Yonkee et al., 1997; DeCelles and Coogan, 2006), where decades of research have yielded a solid understanding of the geometry, magnitude, and timing of deformation (e.g., Lawton, 1983; Lawton et al., 1997; Villien and Kligfield, 1986; Allmendinger, 1992; Burchfiel et al., 1992; DeCelles and Currie, 1996; Yonkee et al., 1997; DeCelles, 2004; Dickinson, 2004; Horton et al., 2004; DeCelles and Coogan, 2006; Yonkee and Weil, 2015). In contrast, within the broad region to the west of the Sevier thrust belt, often referred to as the "Sevier hinterland" (Fig. 1), many uncertainties remain regarding the magnitude, spatial distribution, and timing of Cordilleran contractional deformation (e.g., Taylor et al., 2000; Long, 2015). The paucity of information available for this region is related to multiple factors, including minimal preserved exposures

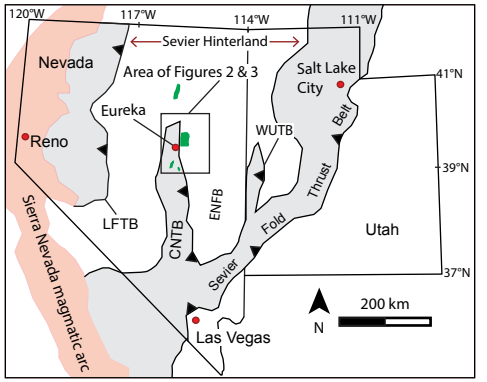

Figure 1. Map showing Cordilleran thrust systems of Nevada and Utah (modified from Long et al., 2014). The approximate spatial extents of Cordilleran thrust systems are shaded, and the Sierra Nevada magmatic arc is shown in red. Exposures of the Cretaceous Newark Canyon Formation are shown in green. Abbreviations: CNTB—Central Nevada thrust belt; ENFB—Eastern Nevada fold belt; LFTB—Luning-Fencemaker thrust belt; WUTB—Western Utah thrust belt.

of Jurassic–Cretaceous synorogenic sedimentary rocks, locally extensive postorogenic Cenozoic cover, and the complex structural overprint of Cenozoic extension.

One debate in the Sevier hinterland focuses on the timing, magnitude, and spatial extent of deformation in the central Nevada thrust belt (CNTB) (Fig. 1), a system of north-striking thrust faults and folds that has been interpreted as an interior component of the Sevier thrust system (Taylor et al., 2000; Long, 2012, 2015; Long et al., 2014). On the basis of crosscutting relationships, the timing of contractional deformation along much of the CNTB can only be broadly bracketed between Permian and Eocene (Nolan, 1962; Taylor et al., 2000). However, in the northern part of the CNTB, there are several isolated exposures of the Cretaceous Newark Canyon Formation (NCF) (Fig. 1). This dominantly clastic unit has long been suspected to be related to regional contractional deformation (e.g., Nolan et al., 1974; Taylor et al., 2000; Druschke et al., 2011; Long et al., 2014) and offers an excellent opportunity to relate deposition directly to motion on thrust faults and the growth of folds.

The goal of this paper is to utilize geologic mapping, structural analysis, and geochronology of the NCF in order to elucidate the geologic evolution of the CNTB at the latitude of Eureka, Nevada (Fig. 2). To achieve this, we present a 1:24,000-scale geologic map focused on exposures of the NCF in the southern Diamond Mountains and U-Pb zircon ages from detrital samples and a waterlain tuff that refine the timing of NCF deposition. We also present field observations that support a scenario of contractional deformation during NCF deposition. We then interpret the implications of these results in the larger context of the spatio-temporal development of the Cordilleran orogenic wedge, by integrating this record of hinterland deformation with the more well-constrained record of shortening in the frontal Sevier thrust belt.

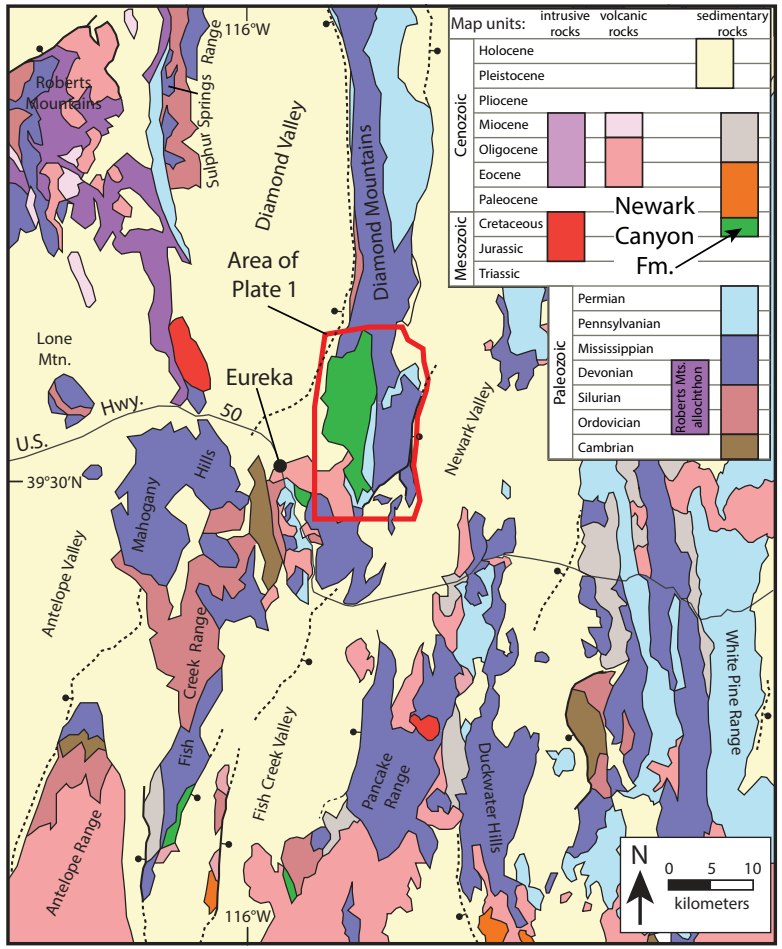

Figure 2. Geologic map of part of east-central Nevada, showing locations and names of ranges and valleys, and the location of the map area of Plate 1 (modified from Long et al., 2014).

CORDILLERAN GEOLOGIC FRAMEWORK

Nevada and western Utah were located along the western margin of the North American continent, which underwent rifting in the Neoproterozoic (e.g., Dickinson, 2006). Rifting resulted in deposition of Neoproterozoic to Lower Cambrian siliciclastic sedimentary rocks within a subsiding, west-facing passive margin basin, followed by shallow-marine deposition of a carbonate-dominated section between the Middle Cambrian and Devonian (Stewart and Poole, 1974; Poole et al., 1992). During the Mississippian, marine slope and basinal sedimentary rocks were thrust eastward over the continental shelf in central Nevada during the Antler orogeny, which has been interpreted as the result of arc-continent collision (Speed and Sleep, 1982; Burchfiel et al., 1992; Poole et al., 1992; Dickinson, 2004, 2006). In response, an associated foreland basin in eastern Nevada filled with ~1.5 km of sediment eroded from the Antler highland to the west (Nolan et al., 1974; Speed and Sleep, 1982;

Poole et al., 1992). Following the Antler orogeny, shallow-marine, carbonate-dominated sedimentation continued in eastern Nevada and western Utah until the Triassic (Stewart, 1980). A cumulative thickness of ~12–15 km of sedimentary rocks was deposited in eastern and central Nevada between the Neoproterozoic and the Triassic (e.g., Stewart, 1980).

During the Middle-Late Jurassic, the closure of a backarc basin in western Nevada resulted in construction of the east-vergent Luning-Fencemaker thrust belt (Fig. 1) (e.g., Oldow, 1984; Wyld, 2002). The closure of this basin was a key step in the consolidation of the western margin of North America into an east-dipping, Andean-style subduction system, which initiated construction of the Cordilleran orogen (e.g., Allmendinger, 1992; Burchfiel et al., 1992; DeCelles, 2004; Dickinson, 2004; Yonkee and Weil, 2015). The Cordillera can be divided into the Sierra Nevada magmatic arc in eastern California and a broad retroarc region across Nevada and western Utah (Fig. 1). In the retroarc region, most of the upper-crustal shortening (~150–220 km) was accommodated by east-vergent, thin-skinned deformation within the frontal Sevier thrust belt in western Utah and southern Nevada (e.g., Lawton et al., 1993; DeCelles and Currie, 1996; Yonkee et al., 1997; DeCelles 2004; DeCelles and Coogan, 2006). In the hinterland region between the Luning-Fencemaker and Sevier thrust belts, three distinct Cordilleran structural provinces have been defined (Fig. 1): the Western Utah thrust belt, Eastern Nevada fold belt, and CNTB. The Western Utah thrust belt accommodated ~10 km of east-vergent shortening and merges southward with the Sevier thrust belt (Greene, 2014). The Eastern Nevada fold belt is characterized by regional-scale, open folds, which are interpreted to have been constructed over the duration of Late Jurassic to Paleocene shortening in the Sevier thrust belt (Long, 2015). The Eastern Nevada fold belt is distinguished from the Western Utah thrust belt and the CNTB by an absence of surface-breaking thrust faults (Gans and Miller, 1983; Long, 2015). The CNTB consists of a series of north-striking, east-vergent thrust faults and folds that branch northward from the Sevier thrust belt in southern Nevada, and it is estimated to have accommodated ~10–15 km of shortening (Taylor et al., 2000; Long et al., 2014). Shortening in the southern part of the CNTB was completed by ca. 85 Ma, on the basis of crosscutting relationships with Late Cretaceous granite bodies (Taylor et al., 2000).

Preserved synorogenic strata within the Sevier hinterland are exceptionally rare. In central Nevada, several scattered exposures of the Cretaceous NCF are the only known synorogenic sedimentary rocks (Figs. 1 and 2). In the northern part of the CNTB, in the region surrounding Eureka, exposures of the NCF are interpreted to have been deposited during regional contractional deformation (Nolan et al., 1971, 1974; Vandervoort and Schmitt, 1990; Carpenter et al., 1993; Druschke et al., 2011; Long et al., 2014), though studies directly linking deposition and deformation of the NCF to motion on specific CNTB structures are lacking.

During the Late Cretaceous and Paleogene, eastern Nevada is interpreted to have been a high (up to ~3 km elevation) orogenic plateau (e.g., Coney and Harms, 1984; DeCelles, 2004; Best et al., 2009; Cassel et al., 2014; Snell et al., 2014), termed the "Nevadaplano" (e.g., DeCelles, 2004). Crustal thicknesses up to 50–60 km are estimated to have been attained in eastern Nevada by the time shortening terminated in the Sevier thrust belt during the Paleocene (Coney and Harms, 1984; DeCelles, 2004; Long, 2019). Despite its high elevation, however, the Nevadaplano experienced minimal synorogenic erosion (up to ~2–3 km) (Long, 2012).

During the Late Eocene and Oligocene, a northeast to southwest migration of magmatism known as the Great Basin ignimbrite flare-up swept across Nevada and is interpreted to be related to post-Laramide rollback of the Farallon slab (e.g., Humphreys, 1995; Best et al., 2009; Smith et al., 2014). During the ignimbrite flare-up, several areas in eastern Nevada experienced localized extension (e.g., Gans and Miller, 1983; Druschke et al., 2011; Lee et al., 2017; Long et al., 2019; Long, 2019). However, paleoaltimetry data indicate that elevations were still high (~2.5–3.5 km) during, and possibly in response to, the ignimbrite flare-up, and therefore the Nevadaplano still existed during the mid-Cenozoic (Cassel et al., 2014).

Most of the widespread extension that constructed the Basin and Range Province, which is the tectonic setting that presently defines this region, took place from the middle Miocene to present (e.g., Dickinson, 2002; Colgan and Henry, 2009; Long, 2019). Basin and Range extension has been attributed to the reorganization of the Pacific–North American plate boundary from an Andean-style subduction system to a continental transform system (e.g., Atwater, 1970; Dickinson, 2002, 2006).

PREVIOUS INTERPRETATIONS OF THE CNTB AND NCF IN THE EUREKA REGION

At the latitude of the town of Eureka (~39°N), CNTB deformation was accommodated by a series of N-striking, E-vergent contractional structures. These include, from west to east, the Eureka culmination, Sentinel Mountain syncline, and Moritz-Nager thrust (Fig. 3). The Eureka culmination is a regional-scale anticline, which is interpreted as a fault-bend fold constructed above a blind thrust that is defined by a Cambrian over Silurian relationship observed in drill holes (Long et al., 2014). Exposed in the western part of the Diamond Mountains, the Sentinel Mountain syncline is an open fold that deforms Devonian–Mississippian rocks (Nolan et al., 1974; Long et al., 2014). The Sentinel Mountain syncline lies in the hanging wall of the Moritz-Nager thrust, which is a steeply W-dipping fault with ~1–2 km of offset that places Devonian rocks over Mississippian rocks (French, 1993; Long et al., 2014).

In the Diamond Mountains, the NCF was originally interpreted to have a Carboniferous depositional age, on the basis of freshwater gastropods (Hague, 1892). Later, MacNeil (1939) assigned these gastropods to the Lower Cretaceous. The name "Newark Canyon Formation" originated from Nolan et al. (1956), who were the first to map the extent of the NCF surrounding Eureka (Nolan et al., 1971, 1974). Following this, Fouch et al. (1979), based on observations of a variety of fossils, including gastropods, bivalves, ostracods, fish, charophytes, angiosperms, and palynomorphs, interpreted an Aptian–Albian deposition age for the NCF. More

recently, using U-Pb dating of zircons from samples collected along the NCF type section in the Diamond Mountains, Druschke et al. (2011) obtained a maximum depositional age of 120.7 ± 3.2 Ma from a sandstone in the middle of the section and a 116 ± 1.6 Ma deposition age from a waterlain tuff higher in the section.

STRATIGRAPHY AND DEPOSITIONAL AGE OF THE NCF

In order to resolve the depositional and deformational history of the NCF, and how it relates to CNTB deformation, we present new 1:24,000-scale mapping (Plate 1), stratigraphic divisions, conglomerate clast compositions, and U-Pb zircon geochronology from two exposures of the NCF in the southern Diamond Mountains (Figs. 2 and 3). The southern of the two exposures, which contains the type section in Newark Canyon as originally defined by MacNeil (1939), is referred to here as the "type exposure" (Fig. 4; Plate 1). To the north of the type exposure, along the western flank of the Diamond Mountains, is a large exposure of the NCF referred to here as the "Hildebrand exposure," which is named after Hildebrand Canyon (Fig. 4; Plate 1).

Lithostratigraphic Divisions

Based on lithologic and stratigraphic relationships observed in our mapping (five members of the NCF were defined), a stratigraphic architecture has been outlined that is broadly consistent between both exposures. While the general lithologic characteristics of these members are consistent throughout the NCF exposures in the southern Diamond Mountains, the different lithofacies within each member are not laterally extensive and often interfinger at the meter-scale. These informal members of the NCF are primarily defined by unique conglomerate clast compositions, in addition to characteristics lithofacies. In the type exposure, the basal member (Knc1) is ~100–120 m thick and is characterized by pebble-rich, dominantly massive micrite and siltstone with interbedded lenses of clast-supported, crudely bedded to cross-stratified, pebble to cobble conglomerate. Conglomerate lenses are ~1–2 m thick and laterally discontinuous (often terminating within ~5–10 m), and they often exhibit convex scoured basal contacts (Fig. 4). Member Knc1 overlies Permian sedimentary rocks across a low-angle (≤~10°) angular unconformity observed on the eastern side of the type exposure. Member Knc1 fines upward into sandstone, siltstone, and silty-sandy micrite of member Knc2, which is ~80–130 m thick. The contact between Knc1 and Knc2 is gradational over an ~3–4 m stratigraphic thickness. Above Knc2, member Knc3 consists of ~110 m of cross-stratified, chert-clast dominant, pebble to cobble conglomerate, with interbedded medium- to coarse-grained, cross-bedded sandstone. Member Knc4, which is only exposed at the northern end of the type exposure, consists of thinly interbedded

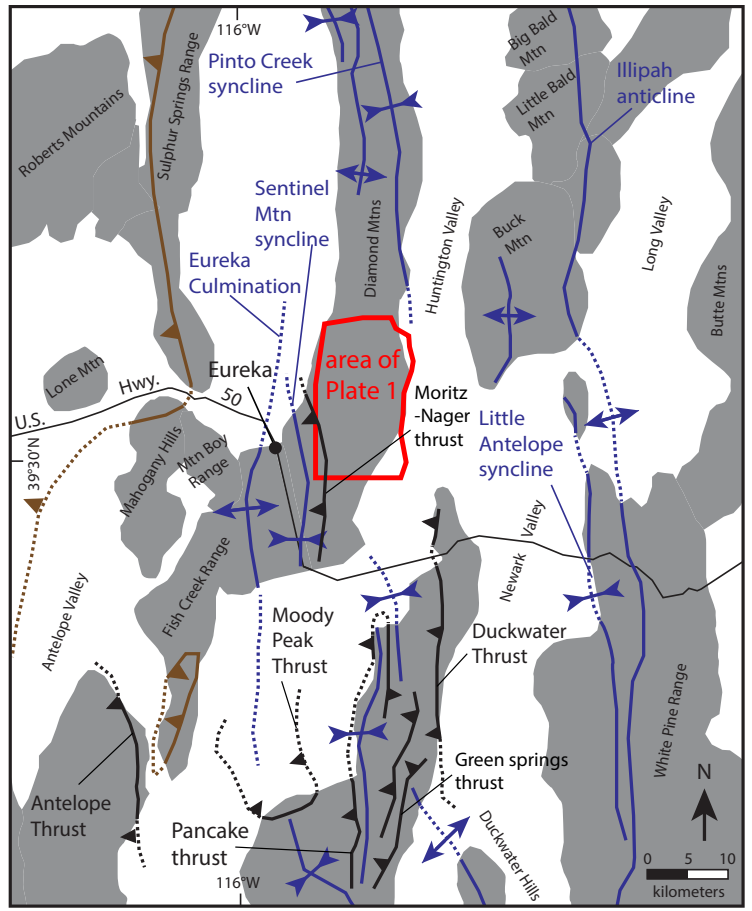

Figure 3. Map of same area as Figure 2, showing locations of Cordilleran folds (in blue) and thrust faults (in black) (modified from Long, 2015). Exposures of the Mississippian Roberts Mountain thrust are shown in brown. Gray shaded areas correspond to ranges, and areas in white are valleys.

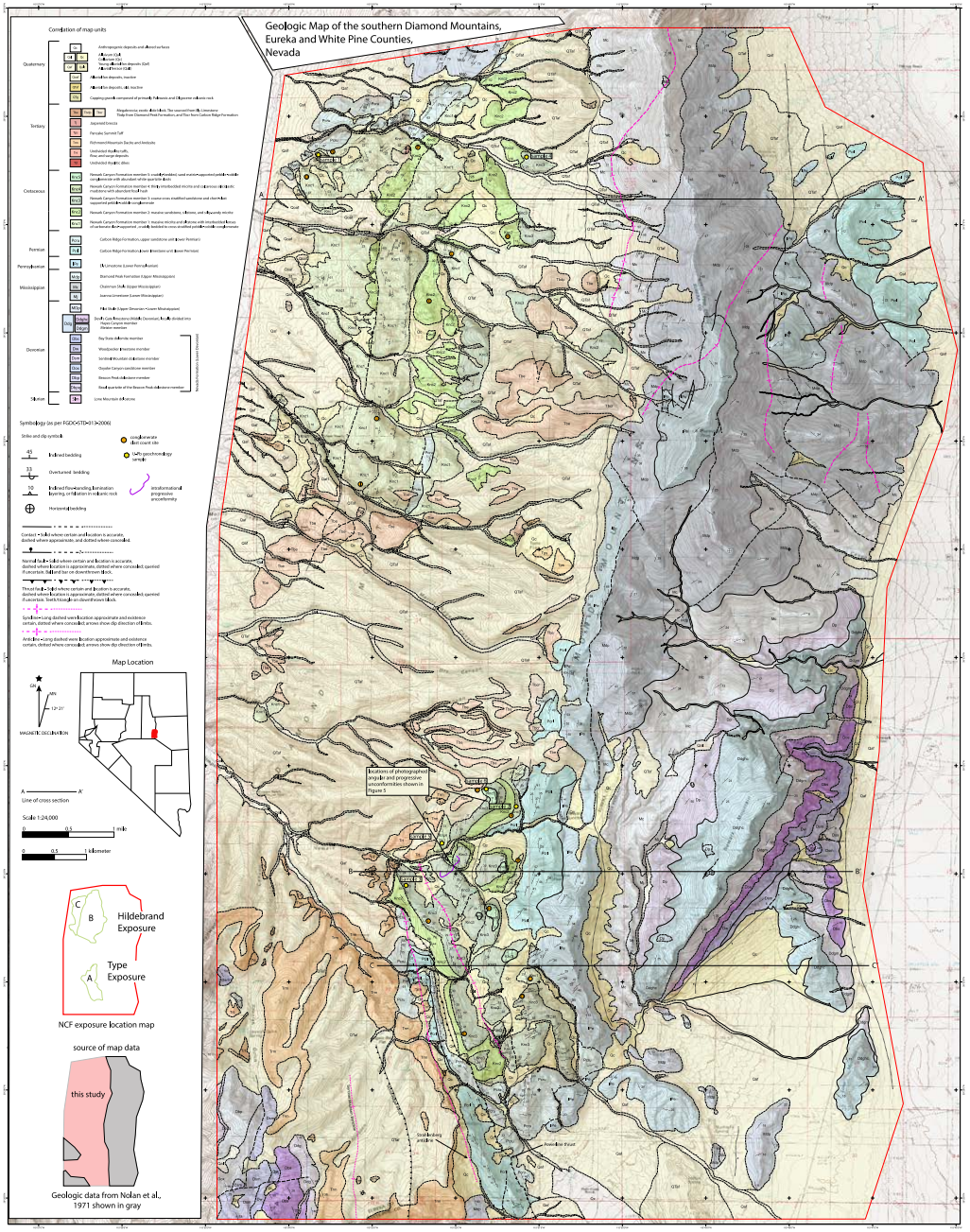

Plate 1. Geologic map (1:24,000 scale) of the southern Diamond Mountains. Newark Canyon Formation (NCF) exposures include the Hildebrand exposure in the north and the type exposure in the south. To view Plate 1 at full size, please visit https://doi.org/10.1130/GES02168.p1 or access the full-text article on www.gsapubs.org.

Plate 1. Geologic map (1:24,000 scale) of the southern Diamond Mountains. Newark Canyon Formation (NCF) exposures include the Hildebrand exposure in the north and the type exposure in the south. To view Plate 1 at full size, please visit https://doi.org/10.1130/GES02168.p1 or access the full-text article on www.gsapubs.org.

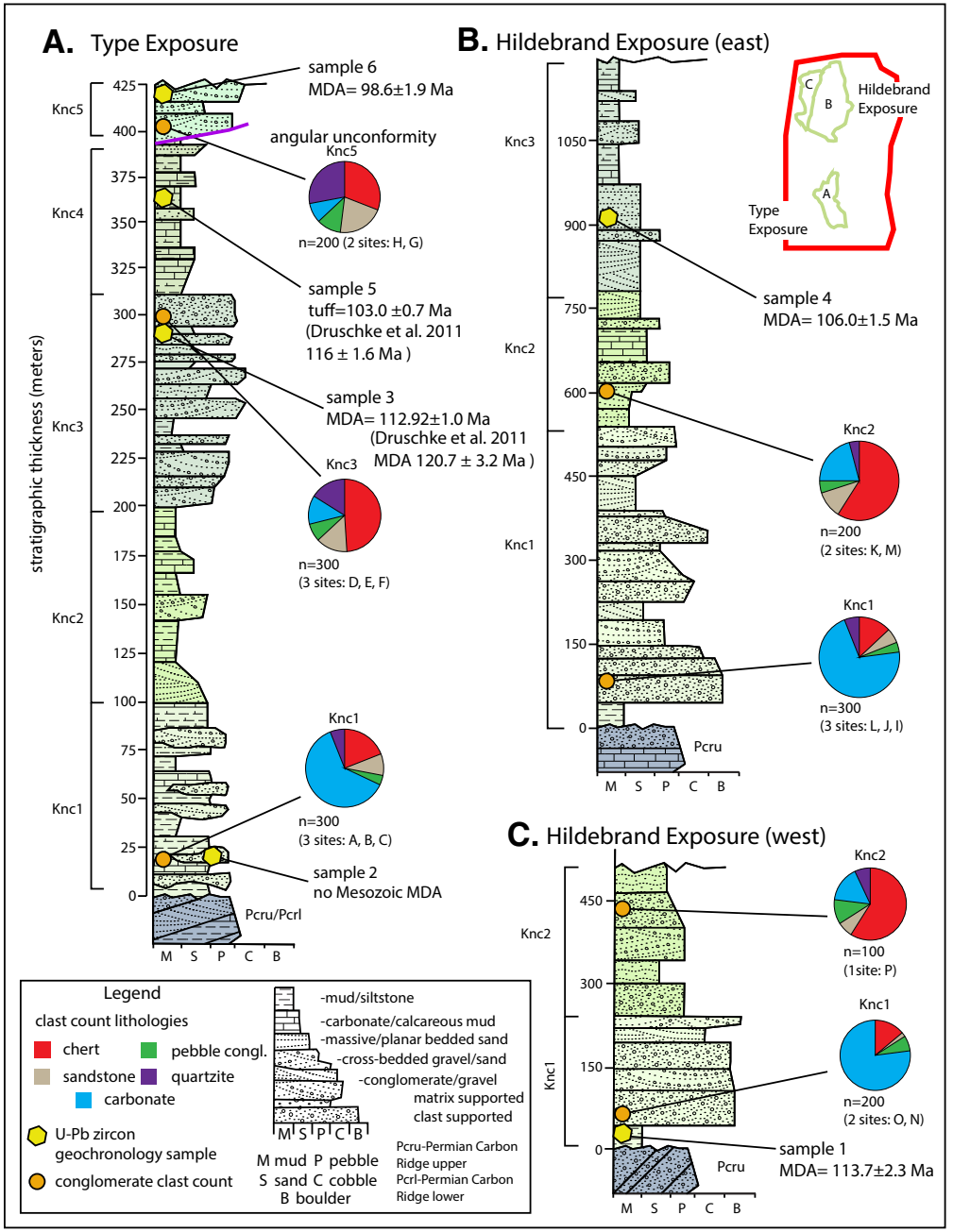

Figure 4. Stratigraphic columns of the Newark Canyon Formation (NCF) in (A) the type exposure and (B-C) the Hildebrand exposure, showing stratigraphic positions of conglomerate clast composition data (and associated pie charts) and U-Pb zircon geochronology samples. MDA is maximum depositional age. Ages from samples from Druschke et al. (2011) are listed with their estimated stratigraphic position.

micrite and calcareous siliciclastic mudstone with abundant fossil hash. A minimum thickness of ~70 m of Knc4 is exposed, and its upper contact is concealed beneath Paleogene volcanic rocks.

In the type exposure, members Knc1 through Knc4 define a conformable section. However, within Knc3, there is evidence for a local progressive (i.e., syndeformational; Riba, 1976) unconformity, where outcrops of ledge-forming conglomerate exhibit a shallower (~17°W) over steeper (~40°W) dip relationship (Fig. 5A). The youngest member in the type exposure is Knc5, which consists of several isolated outcrops of crudely bedded, sand matrix-supported, pebble to cobble conglomerate with abundant quartzite clasts (Fig. 4; Plate 1). Member Knc5 overlies member Knc3 across an angular unconformity with ~10°–20° of difference in dip angle (Fig. 5B), which projects westward above member Knc4. Based on this angular basal contact, distinct clasts of white quartzite, and a significantly younger maximum depositional age obtained from this unit (described in the following section), we interpret Knc5 to be the youngest member of the NCF in the Diamond Mountains. The top of Knc5 is not exposed, and a minimum thickness of ~15 m is preserved.

Vandervoort (1987) collected paleocurrent data from the NCF in the type exposure, using pebble and cobble-clast imbrication and trough long-axis and planar cross-bedding orientations, which yielded a dominant ENE-directed flow direction (average azimuth of ~076°).

To the north, the eastern part of the Hildebrand exposure exhibits a conformable section of Knc members 1–3, which have many lithologic similarities compared to the type exposure, but with a few key differences (Fig. 4). One lithologic difference is that Knc1 lacks micrite in the Hildebrand exposure and instead consists primarily of pebble to cobble, carbonate-clast conglomerate with a distinct basal mudstone. An additional difference is observed in Knc2, which in the Hildebrand exposure is dominated by sandstone and chert-rich pebbly sandstone intervals and lacks the micrite intervals observed in the type exposure. The base of Knc1 is exposed in two places in the eastern part of the Hildebrand exposure, where Knc1 overlies Permian sedimentary rocks across a contact with up to ~20° of dip difference (Plate 1). Members Knc1–3 all exhibit a significant northward thickening between the type exposure and the Hildebrand exposure, with Knc1 thickening from ~100 m to ~400 m, Knc2 from ~100 m to ~250 m, and Knc3 from ~115 m to ≥~420 m (Fig. 6).

On the western side of the Hildebrand exposure, members Knc1 and Knc2 are exposed in the hanging wall of a down-to-the-west normal fault (Plate 1). Knc1 consists of a basal mudstone overlain by clast-supported, cobble conglomerate rich in carbonate clasts; the member is up to ~200 m thick. At the northwestern end of the Hildebrand exposure, Knc1 overlies Permian sedimentary rocks across an angular unconformity (Plate 1). Knc1 is conformably overlain by Knc2, which consists of chert-rich, pebbly sandstone and clast-supported conglomerate, and has a minimum thickness of ~405 m.

U-Pb Zircon Geochronology

In order to obtain more precise constraints on the depositional timing of the NCF, we collected six samples for U-Pb dating of zircon (locations shown on Plate 1); five were detrital samples, while one sample was from a tuffaceous horizon (see Table S1[1] in the Supplemental Material for GPS locations). Sample 1 was collected from a sandstone interval within the basal mudstone of Knc1 in the western part of the Hildebrand exposure. Sample 2 was collected from the matrix of the basal conglomerate of Knc1 in the type exposure. Sample 3 was collected from a coarse-grained sandstone at the top of Knc3 in the type exposure. Sample 4 is from a fine-grained sandstone near the top of Knc3 in the eastern part of the Hildebrand exposure. Euhedral zircons were picked and analyzed from sample 5, which was collected from a reworked waterlain tuff within Knc4 in the type exposure. Sample 6 is from a sandstone horizon within a quartzite-clast conglomerate from Knc5 in the type exposure.

Zircons were obtained by standard mineral separation methods, including crushing, disc grinding, and water table, magnetic, and heavy liquid separation. Zircons were mounted in epoxy resin and polished and cathodoluminescence (CL)-imaged using an electron microprobe at Washington State University (WSU). The zircons were analyzed using laser ablation–inductively coupled plasma mass spectrometry (LA-ICPMS). Analyses were performed at the WSU radiogenic isotope laboratory. This method yields ages with a typical 2-sigma error range of ~1%–2% (e.g., Chang et al., 2006; Gehrels et al., 2008). Between 61 and 151 zircons were analyzed from each detrital sample, and 35 euhedral zircons were analyzed from the waterlain tuff (sample 5). Zircon recovered from all six samples generally consisted of small (~35–150 μm *c*-axis) grains. Grains with visible inclusions and fractures were not analyzed in an effort to avoid potential

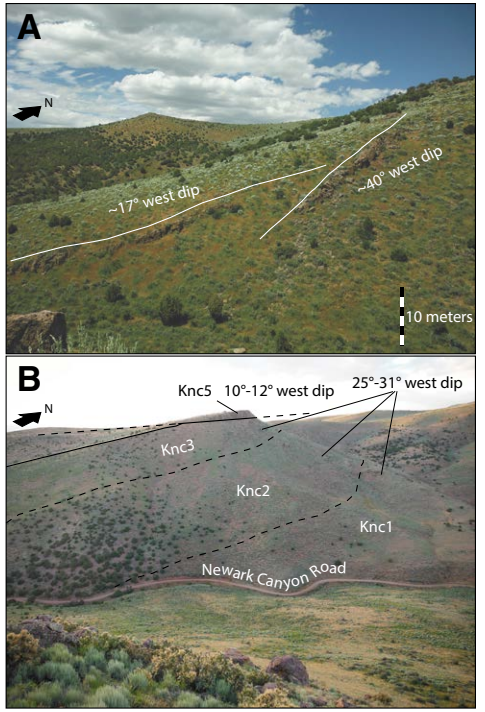

Figure 5. (A) Annotated photograph of progressive unconformity within member Knc3 in the type exposure (facing north). (B) Annotated photograph of the angular unconformity (~15° dip difference) between member Knc5 and the stratigraphically lower members Knc1–3 in the type exposure (facing north-northeast).

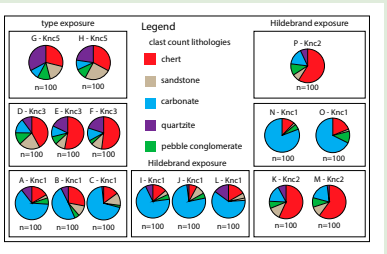

[1]Supplemental Material. Includes geographical information of conglomerate clast-counts and U-Pb zircon sample locations, supporting data for summary conglomerate clast-counts, cathodoluminescent images of igneous zircon from sample 5, and U-Pb zircon geochronology methodology and supporting data set. Please visit https://doi.org/10.1130/GES02168.S1 or access the full-text article on www.gsapubs.org to view the Supplemental Material.

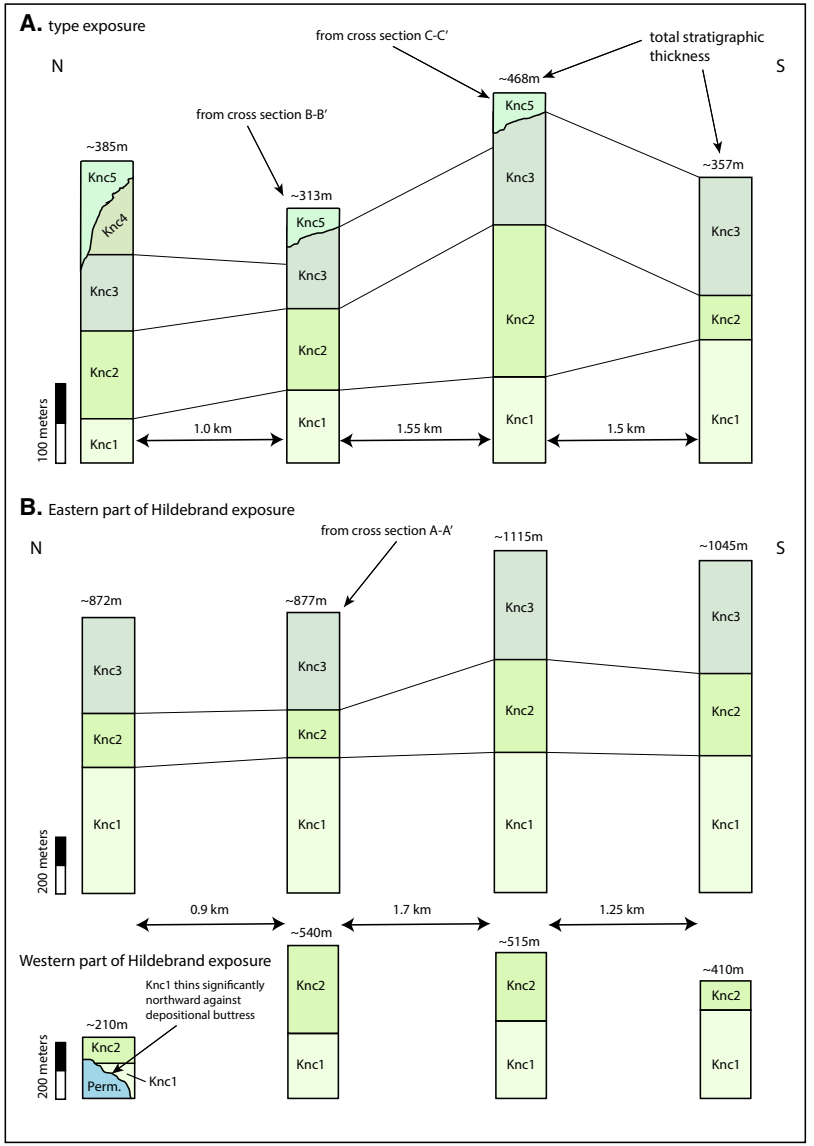

Figure 6. Diagrams showing along-strike (N-S) thickness changes of Newark Canyon Formation (NCF) members between the (A) type, and (B) Hildebrand exposures (note the change in vertical scale between the type exposure and Hildebrand exposure columns). Thickness diagrams for NCF members in the eastern and western parts of the Hildebrand exposure have been separated to show thickness changes across the crest zone of the Strahlenberg anticline. Horizontal arrows show the N-S map distance between stratigraphic thickness columns. Thicknesses of the NCF members were estimated from cross sections where noted and were calculated from map patterns in the other columns.

compromised radiogenic isotope compositions (e.g., Pb-loss). The $^{207}Pb/^{206}Pb$ age was used for grains older than 900 Ma, while the $^{206}Pb/^{238}U$ age was used for grains younger than 900 Ma. Grains that yielded ages 900 Ma and older were allowed up to 15% positive discordance or 5% negative discordance in order to not be discarded, and grains that were younger than 900 Ma but older than 300 Ma were allowed up to 20% positive discordance or 10% negative discordance (Gehrels et al., 2008). Because of the difficulty in calculating discordance for grains younger than 300 Ma, due to the linearity of the concordia curve and the uncertainty of measurement of ^{207}Pb (Bowring and Schmitz, 2003), we allowed 25% positive discordance or 20% negative discordance for grain ages <300 Ma. For the detrital zircon samples, between 15% and 48% of the analyzed grains displayed large uncertainty and/or unacceptable discordance; these analyses were discarded. Using the program Isoplot (Ludwig, 2008), detrital zircon ages were plotted on probability density plots (Fig. 7), and the ages from the tuff (sample 5) were plotted on a concordia diagram (Fig. 8).

We utilized weighted-mean ages of the youngest coherent populations of zircon grains to calculate maximum depositional ages (MDAs) for our five detrital samples. However, among the potential issues inherent in this method is the possibility of unidentified Pb-loss and contamination in the field or laboratory (e.g., Bowring and Schmitz, 2003; Coutts et al., 2019). In an effort to alleviate this issue, we used the weighted-mean age of the five youngest grains that overlap within 1σ uncertainty (the "YC1σ(2+)" or "youngest 1σ grain cluster" method of Dickinson and Gehrels (2009), which was recently interpreted by Coutts et al. (2019) as yielding conservative, but still statistically robust, MDA estimates) to calculate MDAs.

Detrital zircons from sample 1, collected from Knc1 in the Hildebrand exposure, yielded a prominent youngest peak centered at ca. 115 Ma and older peaks at ca. 1.0–1.2 Ga and ca. 1.4–1.6 Ga, with the oldest grains at ca. 2.6–2.7 Ga (Fig. 7). The youngest five overlapping grains from this sample yielded an MDA of 113.7 ± 2.3 Ma. Detrital zircons analyzed from sample 2, collected from Knc1 in the

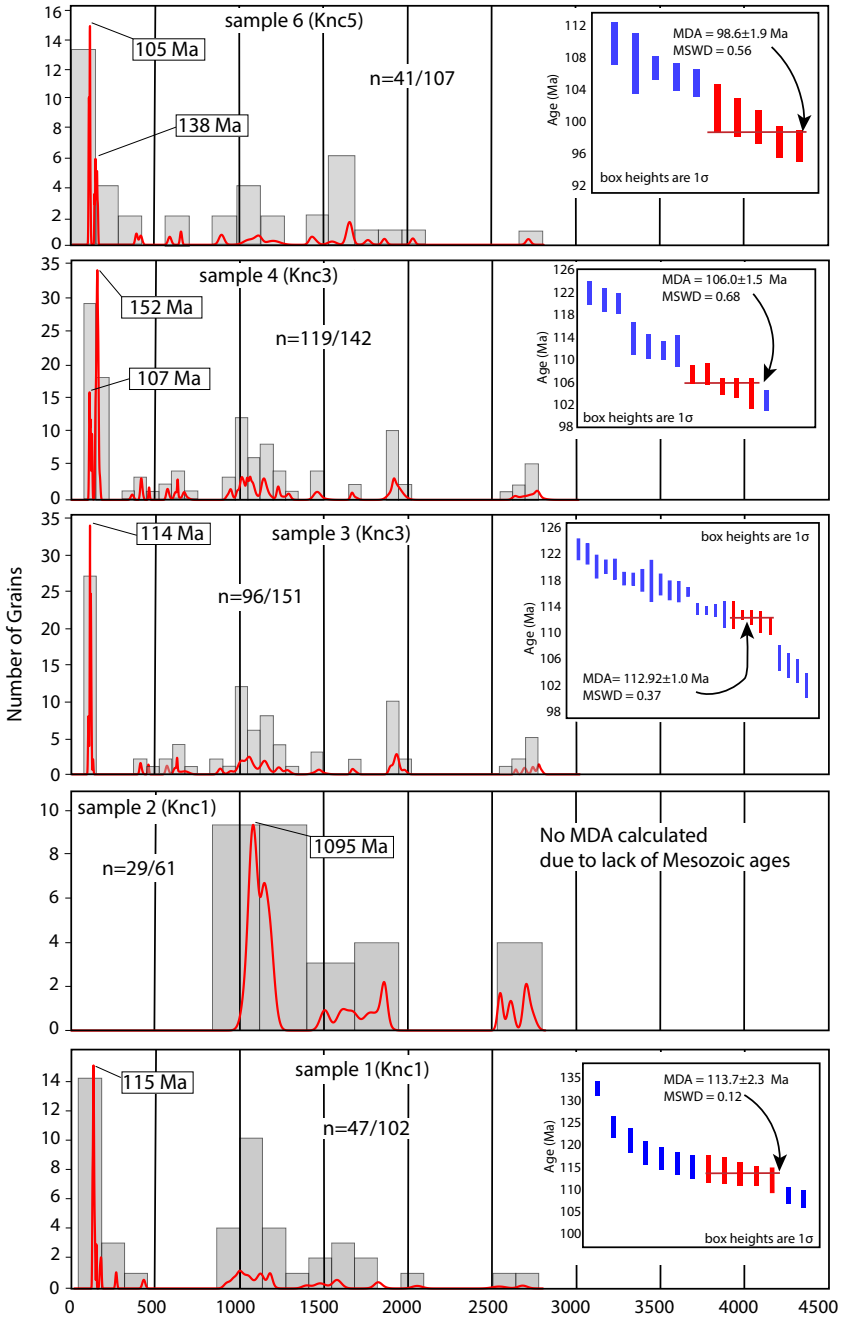

Figure 7. Probability density plots for U-Pb detrital zircon analyses of Newark Canyon Formation (NCF) samples. The center ages of major peaks are labeled (determined in Isoplot; Ludwig, 2008). The number of grains plotted (based on concordance criteria) out of total grains analyzed (e.g., n = 86/150) is shown for each sample. Graphs on the right-hand side show all grain ages that define the youngest age peak for each sample (generated using the zircon age extraction tool in Isoplot; Ludwig, 2008). The weighted-mean age of the five youngest grains that overlap within error (the YC1σ(2+) method of Dickinson and Gehrels, 2009; grains utilized in calculation are highlighted in red) is interpreted as the maximum depositional age (MDA) for each sample and is shown with a red line. No MDA was calculated for sample 2, because it did not yield any Mesozoic zircons. MSWD—mean square of weighted deviates.

type exposure, yielded age groups between ca. 1.0 and ca. 2.8 Ga, including a prominent peak at ca. 1095 Ma, and a series of minor peaks between ca. 1.5 and ca. 1.8 Ga and ca. 2.6–2.7 Ga (Fig. 7). The lack of Mesozoic grains in sample 2 could be due, in part, to poor zircon abundance because this sample was collected from the matrix of a conglomerate horizon. Because no Mesozoic grains were obtained, we did not calculate an MDA for this sample. Detrital zircons from sample 3, collected from Knc3 in the type exposure, yielded a prominent youngest peak centered at ca. 114 Ma, with older age groups between ca. 0.4 and ca. 2.7 Ga, robust peaks at ca. 1.2 Ga and ca. 1.8 Ga, and a small age group at ca. 2.7 Ga (Fig. 7). The five youngest overlapping grains from this sample yielded an MDA of 112.9 ± 1.0 Ma. Detrital zircons from sample 4, collected from Knc3 within the Hildebrand exposure, yielded a youngest peak centered at ca. 107 Ma, a prominent peak at ca. 152 Ma, and older age groups between ca. 0.4 and ca. 2.7 Ga (Fig. 7). The youngest five overlapping grains from this sample yielded an MDA of 106.0 ± 1.5 Ma.

Sample 5 was collected from a lithology interpreted as a reworked waterlain tuff within member Knc4 in the type exposure. This interpretation is supported by the presence of tricuspid volcanic glass shards within the sample, which suggests minimal reworking after deposition of the tuffaceous component. Additionally, this same interval was also interpreted as a waterlain tuff by Druschke et al. (2011). Thirty-five >100 μm *c*-axis euhedral zircons from this sample were analyzed (see supporting

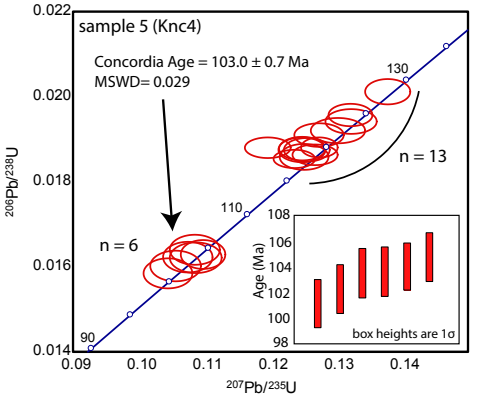

Figure 8. Concordia plot for sample 5, a waterlain tuff collected from member Knc4 within the type exposure (generated in Isoplot; Ludwig, 2008). The youngest six grains define a concordant, overlapping age group, and were used to determine a concordia age of 103.0 ± 0.7 Ma (1σ). The inset graph on the lower right shows the age ranges of the six grains that were used to calculate the concordia age. MSWD—mean square of weighted deviates.

information for a CL image), 16 of which were discarded for exceeding the defined discordance cutoff. The resulting ages are clustered into two age groups (Fig. 8), with the youngest six grains defining a coherent, overlapping population with a concordia age of 103.0 ± 0.7 Ma, and the oldest 13 grains defining a distribution of ages between ca. 115 and ca. 130 Ma. We interpret the 103.0 ± 0.7 Ma age of the youngest group to represent the actual age of deposition of Knc4. The older age group of zircons (ca. 115–130 Ma) could be the result of older in situ zircon evacuated by a younger eruptive event from the same eruptive center, or perhaps from incorporation of older zircons from erosion of underlying NCF members. This same tuffaceous horizon was also dated by Druschke et al. (2011), who obtained a youngest age group of zircons centered at 116 ± 1.6 Ma.

Finally, detrital zircons from sample 6, collected from Knc5 in the type exposure, yielded a prominent peak centered at ca. 105 Ma, and a series of smaller peaks distributed between ca. 0.4 and ca. 2.7 Ga, with a prominent peak at ca. 1.2 Ga (Fig. 7). The youngest five overlapping grains yielded an MDA of 98.6 ± 1.9 Ma.

In summary, our new U-Pb ages indicate that deposition of the basal member of the NCF (Knc1) occurred no earlier than ca. 114 Ma, deposition of member Knc3 occurred no earlier than ca. 106 Ma, Knc4 was being deposited at ca. 103 Ma, and deposition of the youngest member (Knc5) occurred no earlier than ca. 99 Ma. Therefore, deposition spanned from possibly as early as the late Aptian until at least the early Cenomanian.

STRUCTURAL GEOMETRY OF NCF EXPOSURES

In this section, the deformation geometry of the two NCF exposures, as well as proximal areas of the Diamond Mountains, are described. This discussion is supported by three cross sections (Figs. 9–11; lines of section shown on Plate 1).

Type Exposure

In the type exposure, the NCF is folded into an open, E-vergent syncline with a steeply dipping (~60–90°E, but locally overturned) western limb and an eastern limb that dips moderately (~25°) to the west (Figs. 9 and 10). The western limb lies in the footwall of a previously unmapped, ~60° W-dipping, top-to-the-E reverse fault, here named the "Powerline thrust." The Powerline thrust places Permian rocks in its hanging wall against Knc2 in its footwall, defining an older-over-younger relationship. In the hanging wall of the Powerline thrust, Permian rocks are deformed into an E-vergent anticline, here named the "Strahlenberg anticline," which has a ~60°–90°–dipping eastern limb and a ~40°–50°–dipping western limb (Figs. 9 and 10). The basal unconformity of the NCF on the eastern side of the type exposure overlies Permian rocks and exhibits a minimal (~0°–10°) difference in dip angle (Figs. 9 and 10).

When displacements on normal faults are retro-deformed and the basal NCF unconformity in the eastern limb of the syncline is restored to horizontal (Figs. 9B and 10B), the overall deformation geometry defines the asymmetric Strahlenberg anticline with a steeply dipping (~80° E) eastern limb. Based on this geometry, we interpret that this anticline was most likely constructed as a fault-propagation fold (e.g., Suppe and Medwedeff, 1990) above an E-vergent thrust fault that tips out in the subsurface (Figs. 9 and 10). We interpret that the Powerline thrust represents a small-offset (~100 m), high-angle breakthrough thrust fault (e.g., Suppe and Medwedeff, 1990, their figure 11E) that branches upward from the blind thrust at depth. Based on our interpreted subsurface geometry, the blind thrust may root westward into a flat within Mississippian rocks. The Mississippian section consists dominantly of shale and sandstone, with a lesser abundance of conglomerate and thin-bedded limestone. The rheological contrast between the Mississippian clastic units, in particular the Mississippian Chainman shale in the lower part of the section, and the thick-bedded carbonates of the overlying Pennsylvanian–Permian section and underlying Devonian section, provides an ideal weak stratigraphic interval for exploitation as a detachment horizon. The approximate depth to the detachment is constrained by the geometry of the fault-propagation fold, specifically the structural height of the steep forelimb (e.g., Suppe and Medwedeff, 1990, their figure 11E).

Normal faulting overprints all contractional structures in the map area (Figs. 9–11; Plate 1). The normal faults in the map area are difficult to precisely date using crosscutting relationships. However, several down-to-E normal faults on the eastern flank of the Diamond Mountains are interpreted to be related to the Neogene subsidence of adjacent Newark Valley (Figs. 2 and 3) (e.g., Nolan et al., 1971, 1974). Tilting accompanying motion on these normal faults is interpreted as the most likely mechanism for producing the westward dips observed in the eastern limb of the syncline within the NCF type exposure. However, it is also possible that some of this tilting accompanied regional contractional deformation in the CNTB, including the growth of folds to the east of the map area (e.g., Long, 2015).

Hildebrand Exposure

The Hildebrand exposure can be divided into western and eastern domains that are separated

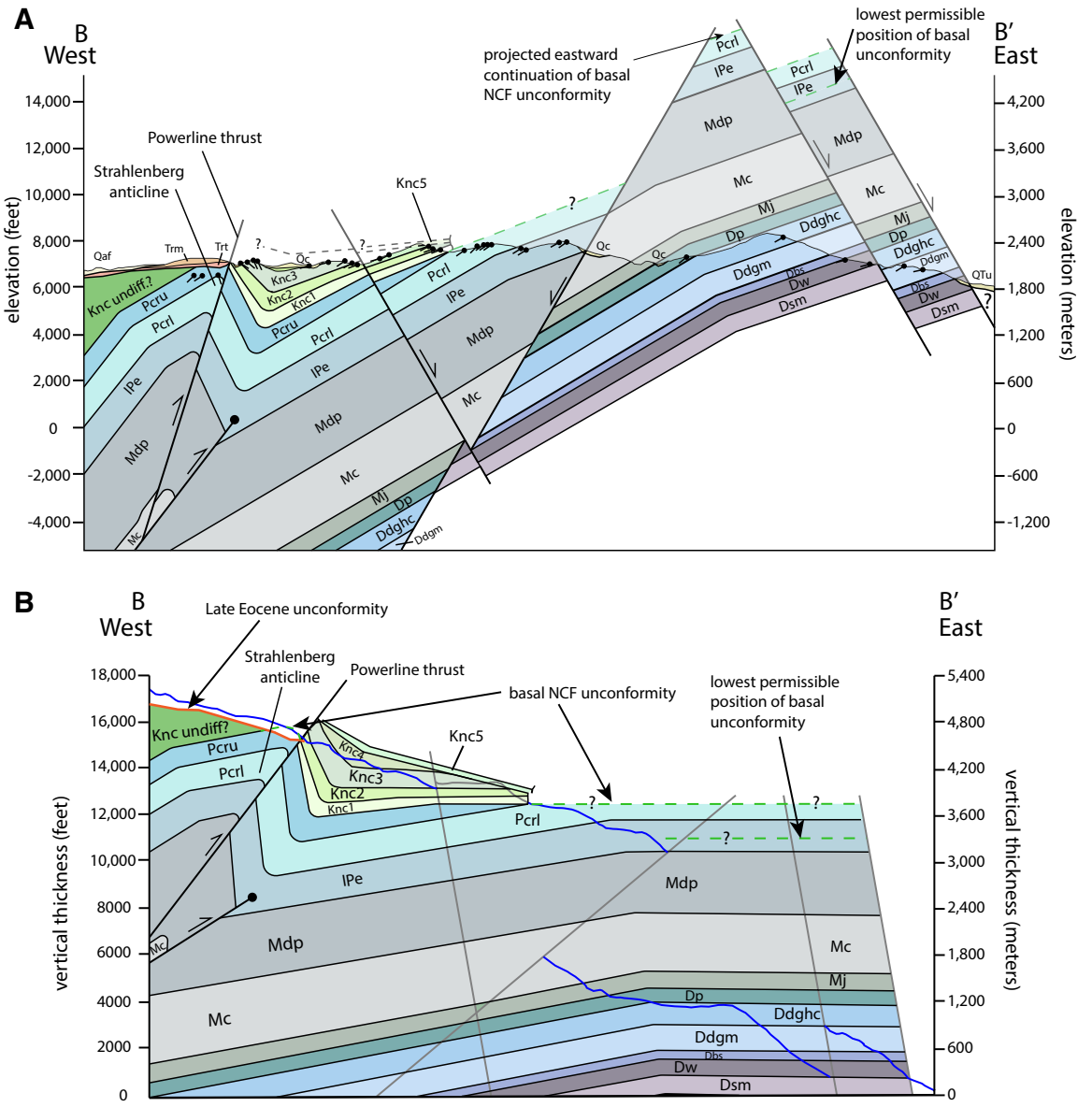

Figure 9. (A) Cross section B–B′ through the type exposure. See Plate 1 for a guide to unit abbreviations. (B) Cross-section B–B′ with motion on normal faults restored, and ~20° of westward tilting of the basal Newark Canyon Formation (NCF) unconformity (as recorded in the eastern limb of the syncline that deforms the NCF) restored. Blue lines indicate the modern erosion surface. The projected level of the basal NCF unconformity on the eastern end of the cross section is unknown; the lowest permissible level of the unconformity, as constrained by modern exposures of Pennsylvanian rocks ~2 km to the south of the map area (Long et al., 2014), is labeled.

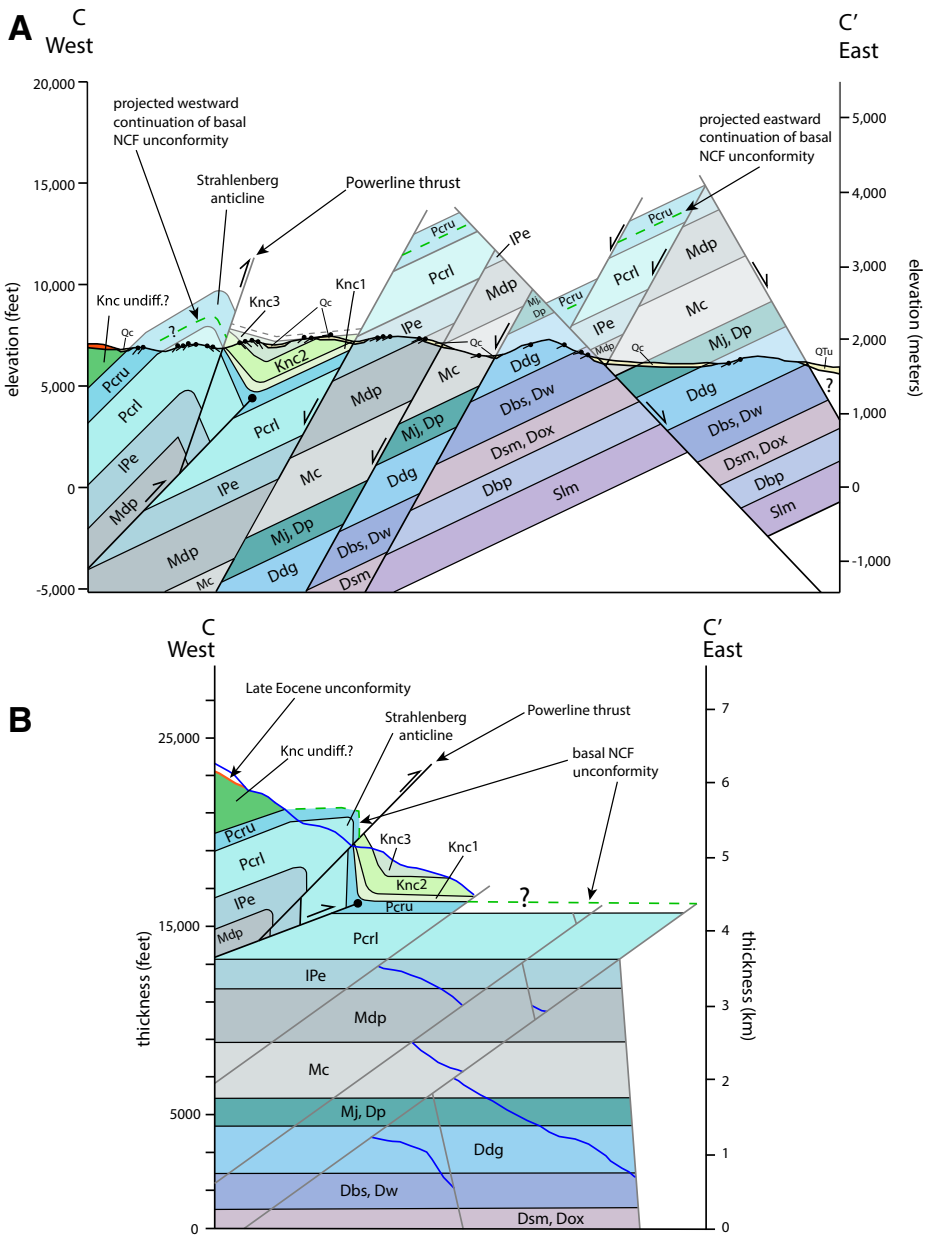

Figure 10. (A) Cross-section C–C′ through the type exposure. See Plate 1 for a guide to unit abbreviations. (B) Cross-section C–C′ with motion on normal faults restored, and ~30° of westward tilting of the basal Newark Canyon Formation (NCF) unconformity (as recorded in the eastern limb of the syncline that deforms the NCF) restored. Blue lines indicate the modern erosion surface.

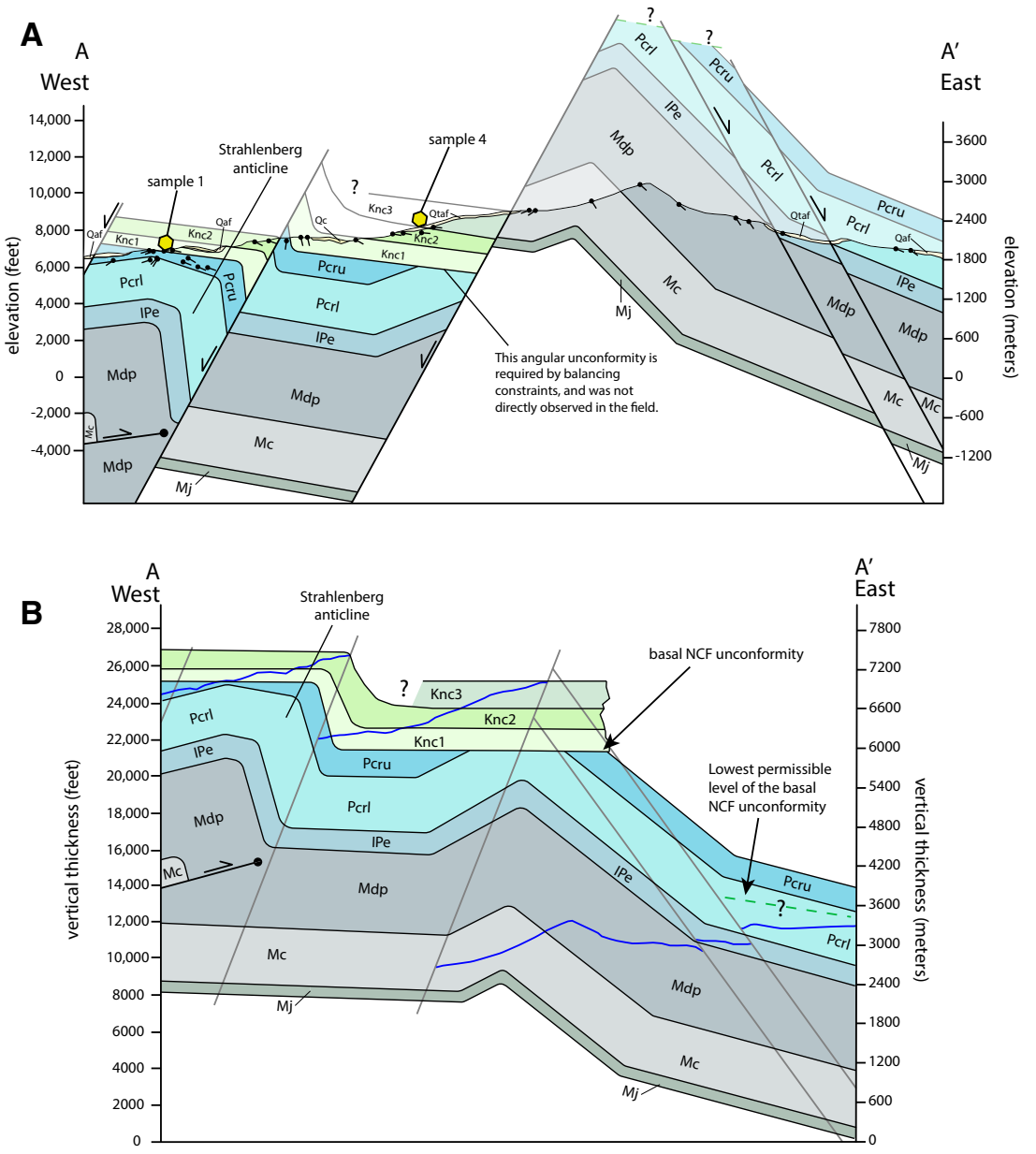

Figure 11. (A) Cross section A–A′ through the Hildebrand exposure. See Plate 1 for a guide to unit abbreviations. (B) Cross-section A–A′ with motion on normal faults restored, and ~8° of eastward tilting of the basal Newark Canyon Formation (NCF) unconformity restored. Blue lines indicate the modern erosion surface. The projected level of the basal NCF unconformity on the eastern end of the cross section (and its magnitude and direction of tilting) is unknown; so the lowest permissible level of the unconformity, as constrained by modern exposures of Permian rocks, is labeled.

by a N- to NNE-striking, down-to-W normal fault (Fig. 11; Plate 1). On the west side of the fault, Knc1 and Knc2 dip moderately (~20°–30°) to the east. On the east side of the fault, a steeply E-dipping (locally vertical to overturned) section of Knc1 gradually shallows in dip angle to the east, and transitions into a gently (~10°–20°) E-dipping section of members Knc2 and Knc3. In the eastern part of the Hildebrand exposure, Permian rocks are observed below the basal NCF unconformity in two places, lying below Knc1 across a contact with minimal difference in dip angle (Plate 1). On the northwestern end of the exposure, folded Permian rocks underlie Knc1 across an unconformity with up to ~20° of difference in dip angle (Fig. 11). On the eastern edge of the exposure, the NCF is cut by a down-to-west normal fault with ~1.2 km of offset that bounds the western side of the Diamond Mountains (Fig. 11; Plate 1).

Similar to the type exposure, we interpret that the structural geometry of the Hildebrand exposure can be most easily explained by growth of the E-vergent Strahlenberg anticline (Fig. 11). In our subsurface interpretation, the steeply E-dipping section of Permian rocks and Knc1 lie in the forelimb, and the gently E-dipping section of Permian rocks and Knc1 and Knc2 on the western edge of the exposure lie in the back limb. Knc1 and Knc2 are thinner above the crest zone of the Strahlenberg anticline than they are in the forelimb (Figs. 6 and 11), which implies deposition during folding.

To the east of the Hildebrand exposure, in the Diamond Mountains, there is additional evidence for folding that predates NCF deposition. An open anticline is observed in Mississippian rocks, and exposures of Knc2 and Knc3 that project over its western limb exhibit a consistent eastward dip (Fig. 11; Plate 1). Balancing constraints, including the lack of westward dips observed in Knc2 and Knc3, require an angular unconformity at the base of the NCF over the western limb of the anticline. This indicates that the Diamond Mountains were subjected to some contractional deformation and erosion prior to NCF deposition. This is consistent with observations of folds distributed across eastern Nevada that in most places can only be bracketed as post-Permian or post-Triassic (Long, 2015), including several folds documented farther to the north in the Diamond Mountains (Larsen and Riva, 1963; Nolan et al., 1971).

ADDITIONAL OBSERVATIONS SUPPORTING SYNCONTRACTIONAL DEPOSITION OF THE NCF

In addition to the details on the structural geometry of the NCF exposures described above, the following field relationships also support a scenario of deposition of the NCF during the progressive growth of folds in the Diamond Mountains:

1. Progressive Unconformity within Knc3

In the eastern limb of the syncline in the NCF type exposure, ledge-forming conglomerate beds within Knc3 exhibit an intraformational, shallow (~17°W dip) over steep (~40°W dip) bedding relationship (Fig. 5A; Plate 1). This angular relationship is interpreted as the result of active sedimentation during progressive growth of the syncline in the type exposure and the associated Strahlenberg anticline to the west. We interpret this relationship to be indicative of growth strata within the NCF, because it is preserved within a single member (Knc3), which likely represents a minimal time lapse across the angular contact. In contrast, the angular unconformity at the base of member Knc5 (described below) is not interpreted to represent a growth relationship, because this contact separates different members (Knc5 from Knc2–4), thus indicating a substantial hiatus.

2. Angular Unconformity at the Base of Knc5

In the type exposure, five separate outcrops of Knc5, distributed over a N-S distance of ~4.5 km, consistently exhibit a westward dip that is between ~10°–20° shallower than the homogeneously W-dipping section of Knc1–3 below (Figs. 5B and 9; Plate 1). This angular unconformity, when combined with the U-Pb zircon geochronology presented above that requires Knc5 to have been deposited at least ~4 m.y. after deposition of Knc 4, is interpreted as the result of NCF deposition spanning the long-term growth of the syncline in the type exposure and associated Strahlenberg anticline to the west.

3. Unroofing Sequence Recorded in Clast Compositions of NCF Conglomerate

To provide information on the source rocks that were being eroded during NCF deposition, clast composition counts (e.g., Dickinson, 1974, 1988; DeCelles, 1994; Horton et al., 2004) were performed from both NCF exposures (Fig. 4; Plate 1). Clast counts were performed at 16 conglomerate outcrops from all NCF members except for the carbonate-dominated Knc4 (locations of individual clast count sites are shown on Plate 1, GPS locations of each site are listed in Table S1 [footnote 1] in the Supplemental Material, and data from individual clast counts are shown in Figure S1 in the Supplemental Material). In each analysis, 100 clasts that were each ~3 cm or larger in diameter were counted within a ~1 m^2 area. Clast lithology categories included chert, carbonate, sandstone, quartzite, and pebble conglomerate. It is likely that less competent lithologies such as mudstone and fine-crystalline carbonate are under-represented in our clast counts, while more competent lithologies such as quartzite and chert may be over-represented due to respective differential weathering. The clast count data are shown in pie charts on Figure 4, with counts from each NCF member in each exposure combined into a single pie chart.

The clast populations from Knc1 are dominated (~62%–77% range) by coarse-crystalline, fossil-bearing carbonate clasts (Fig. 4). Many clasts contain fusilinids and brachiopods, which we interpret to have been sourced from Pennsylvanian–Permian carbonates. Members Knc2 and 3 yielded clast compositions dominated (~49%–59% range) by sub-rounded chert clasts, and member Knc5 exhibits a robust population (~28%) of white quartzite clasts (Fig. 4).

We interpret the fusilinid- and brachiopod-bearing carbonate clasts from member Knc1, which directly overlies Permian rocks, to have been

derived from erosion of proximal Pennsylvanian to Permian, post-Antler, passive margin carbonates (Fig. 12). The chert-rich clast populations from members Knc2 and 3 are interpreted to have been sourced from erosion of proximal Mississippian sedimentary rocks of the Antler foreland basin; these rocks contain chert-rich conglomerates originally derived from erosion of the Roberts Mountains allochthon to the west (e.g., Nolan et al., 1974). The white quartzite clasts in member Knc5 are interpreted to have been derived from erosion of the proximal Devonian section, which contains two white quartzite units (the Oxyoke Canyon Sandstone and the basal quartzite of the Beacon Peak member of the Nevada Formation; e.g., Nolan et al., 1974). We cannot rule out erosion of the Ordovician Eureka quartzite as a potential source, though we consider erosion of the stratigraphically higher Devonian section more likely due to limited syn-Cordilleran erosion in this region of Nevada (e.g., Long, 2012).

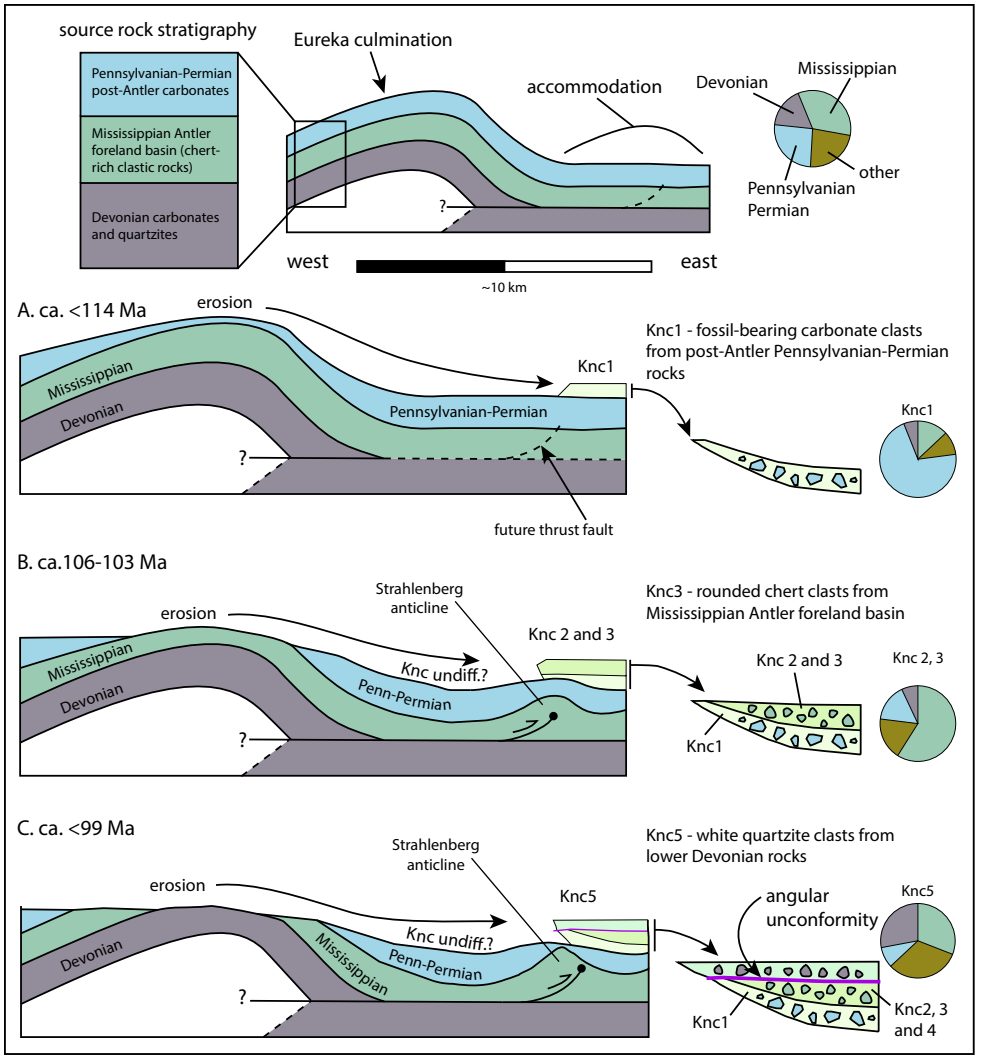

Figure 12. Simplified diagrams illustrating the unroofing sequence recorded in Newark Canyon Formation (NCF) conglomerate clast compositions. Time intervals A, B, and C correspond to deposition of the specified NCF members. Pie charts show Paleozoic source unit interpretations of clast lithologies.

Based on these clast provenance interpretations, the NCF clast composition data define a three-part unroofing sequence, recording progressively deeper levels of the Paleozoic section being unroofed during NCF deposition. We interpret that the simplest scenario that explains this data is the growth and progressive erosional denudation of the crest zone of the Eureka culmination, which was located ~10–15 km to the west of the NCF exposures (Fig. 12). This regional-scale anticline, which was structurally elevated as much as ~4–5 km relative to the surrounding region, has been previously interpreted to have been constructed during NCF deposition (Long et al., 2014). Mapping ~10 km to the southwest of our map area shows that rocks as young as Permian are preserved in the eastern limb of the culmination, indicating that these rocks were still preserved at the surface during initial fold growth (Long et al., 2014). Erosion of its crest zone would have progressively exhumed deeper Paleozoic stratigraphic levels through time, from Permian–Pennsylvanian carbonates, to Mississippian chert-rich clastics, to Devonian rocks that contain white quartzite. This unroofing is inversely reflected in the bottom-up NCF member stacking order (Fig. 12) and provides a record of localized erosion, transport, and deposition associated with CNTB deformation at this latitude.

4. Along-Strike Thickness Changes in NCF Members

Stratigraphic thicknesses (as measured from map patterns and cross sections) exhibit significant along-strike variations over short map distances

(Fig. 6), both for individual NCF members and for the cumulative thickness of the NCF section. In the type exposure, the NCF reaches a maximum preserved thickness of ~525–600 m, and in the Hildebrand exposure the preserved thickness is as much as ~870–1045 m. Within the type exposure, over a N-S distance of ~5 km, Knc1 increases in thickness southward from ~55 to ~160 m, Knc2 varies between ~65 and ~115 m-thick, and Knc3 varies between ~95 and >~185 m thick. In the Hildebrand exposure, Knc1 and 2 are cumulatively thicker (~635 m) in the forelimb of the Strahlenberg anticline and thin (~450 m) to the west over its crest zone. In the northwestern part of the Hildebrand exposure, the entire ~240 m thickness of Knc1 thins abruptly across a buttress unconformity with Permian rocks (Plate 1). We interpret these thickness differences as the likely result of changes in accommodation magnitude that were controlled by the growth of the Strahlenberg anticline and proximal CNTB structures to the west, such as the Moritz-Nager thrust.

DISCUSSION

Interpretations of NCF Basin Evolution and Relationship to Regional CNTB Deformation

Syntectonic basins offer important records of the processes and timing of deformation within orogenic belts (e.g., Dickinson, 1974, 1988). Here, we synthesize the observations and data presented above to generate a model that describes the evolution of NCF deposition and associated CNTB contractional deformation in the southern Diamond Mountains.

The progressive unconformity within Knc3 in the type exposure (Fig. 5A), as well as the angular unconformity between Knc3 and Knc5 (Fig. 5B), are interpreted as the result of active NCF sedimentation over the duration of construction of the Strahlenberg anticline. The angular contact between Knc3 and Knc5 represents both a depositional hiatus and evidence for folding between deposition of these two members. We interpret that uplift of the crest zone of the Strahlenberg anticline, and accompanying subsidence of its eastern limb, was the primary mechanism for generating accommodation space (Fig. 13). The NCF was progressively deposited by sedimentary infilling within the topographic low generated to the east of the Strahlenberg anticline. The minimum amount of accommodation space created by folding can be estimated by the cumulative thickness of the NCF, which varies between ~525 m in the type section and ~1045 m in the Hildebrand exposure. The deposition of Knc1 and Knc2 over the crest zone of the Strahlenberg anticline (Fig. 11), clast compositions that indicate progressive erosional unroofing from Permian down to Devonian stratigraphic levels (Fig. 12), and east-directed paleocurrents (Vandervoort, 1987) indicate that the NCF was likely sourced from erosion of topographically uplifted areas to the west. This uplift was likely generated by motion on the Moritz-Nager thrust and growth of the Eureka culmination (Fig. 13).

Conglomerate-clast composition data from the NCF record the progressive unroofing of the source area to the west, from Pennsylvanian–Permian stratigraphic levels during deposition of Knc1, to Mississippian levels during deposition of Knc2 and Knc3, to Devonian levels during deposition of Knc5 (Figs. 12 and 13). We interpret that growth and accompanying erosional denudation of the Eureka culmination ~10–15 km to the west (Long et al., 2014) is the most likely scenario that explains these clast count data. Therefore, we interpret that the NCF was sourced locally, and represents proximal deposition to the east of the Eureka culmination, with the geometry of the depocenter controlled by smaller-offset CNTB structures including the Moritz-Nager thrust and Strahlenberg anticline. This anticline is interpreted as an E-vergent fault-propagation fold that formed above a blind thrust fault that likely roots westward into a flat in Mississippian rocks. In the type exposure, the forelimb of the Strahlenberg anticline has been breached by the Powerline thrust, a steeply W-dipping fault with ~100 m of offset.

An approximate shortening estimate can be calculated by compiling displacement magnitudes on CNTB contractional structures that are proximal to the NCF in the Diamond Mountains (Plate 1). Construction of the Strahlenberg anticline and motion on the associated Powerline thrust are estimated here to have a total of ~2.5 km of top-to-east displacement (Figs. 9 and 10). To the west, the Moritz-Nager thrust has an estimated top-to-east displacement of ~1.0–1.8 km, and the Eureka culmination was interpreted to have been constructed by ~9 km of top-to-east displacement on the blind Ratto Canyon thrust (Long et al., 2014). Together, these structures account for ~12.5–13.3 km of shortening (~18%) in the CNTB at this latitude.

Our new U-Pb zircon timing constraints have significantly revised the depositional history of the NCF at this latitude. Our geochronology indicates that deposition of the basal mudstone of Knc1 took place no earlier than ca. 114 Ma, Knc3 deposition occurred no earlier than ca. 106 Ma, deposition of Knc4 was under way at ca. 103 Ma, and deposition of Knc5 occurred no earlier than ca. 99 Ma. These new U-Pb zircon age data provide new information on the timing and duration of contractional deformation within the CNTB at this latitude; this new information can be placed in the larger framework of the space-time patterns of strain accommodation within the Cordilleran orogen.

Implications of CNTB Timing for Strain Partitioning within the Cordilleran Orogenic Wedge

To the east in Utah, the Sevier thrust belt accommodated upper-crustal shortening over the duration of Cordilleran orogenesis, spanning from the latest Jurassic to the Paleocene (e.g., DeCelles, 2004; Yonkee and Weil, 2015). The Sevier thrust belt is characterized by an overall forward-breaking sequence of east-vergent thrust faults, punctuated by episodic out-of-sequence thrust reactivation and culmination growth (e.g., DeCelles et al., 1995; Currie 2002; DeCelles and Coogan; 2006). The Sevier thrust belt is characterized by initial emplacement of a thick, spatially extensive, western thrust sheet, which carries an ~10–15-km-thick section of Neoproterozoic–Mesozoic sedimentary rocks that were deposited west of the Wasatch hingeline (e.g., Yonkee and Weil, 2015). Emplacement of this extensive thrust sheet was followed by emplacement of multiple, thinner, smaller-offset thrust sheets toward the

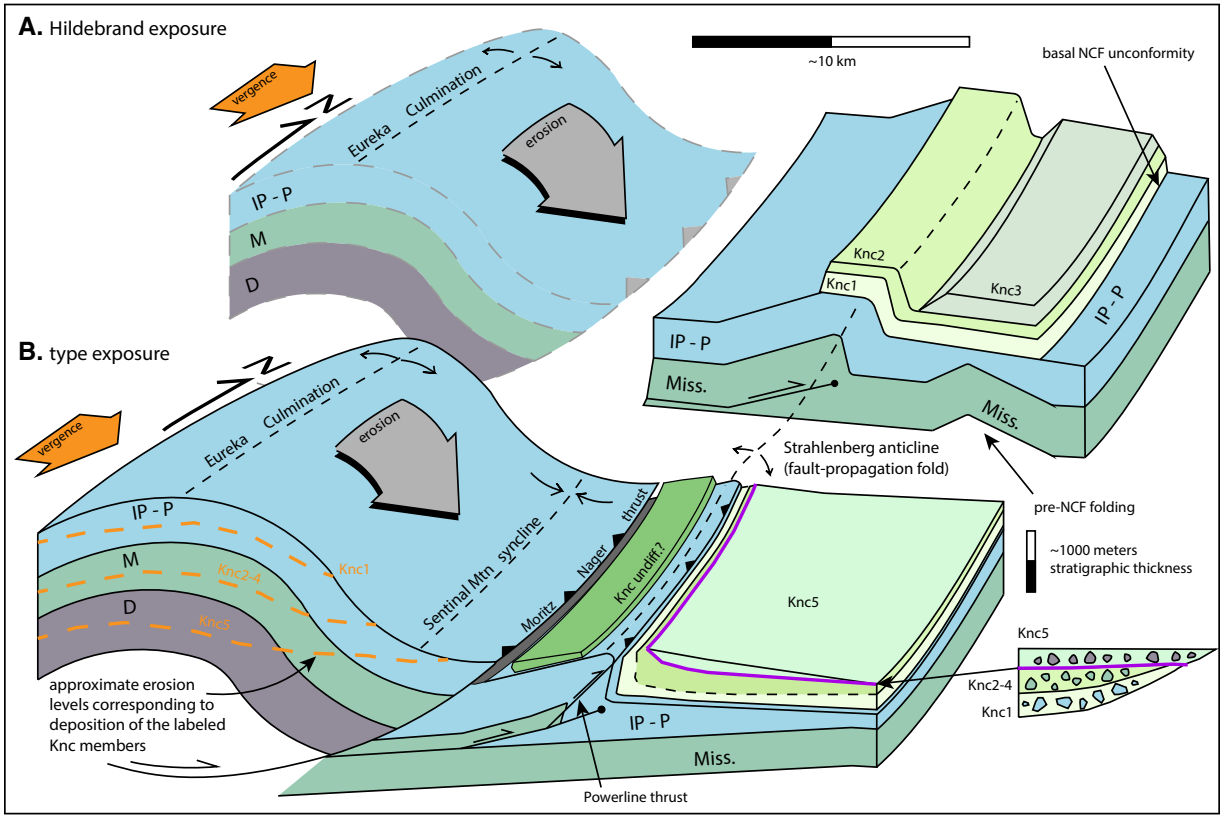

Figure 13. Simplified structural block models of Central Nevada thrust belt contractional deformation and Newark Canyon Formation (NCF) deposition in (A) the Hildebrand exposure, and (B) the type exposure. The Eureka culmination west of the Hildebrand block model is shown as translucent due to the lack of bedrock exposure to the west in Diamond Valley. All normal faults have been omitted for simplicity. IP-P—Pennsylvanian–Permian; M, Miss.—Mississippian; D—Devonian.

foreland; these sheets deform an ~2–5-km-thick section of Paleozoic–Mesozoic sedimentary rocks that were deposited to the east of the Wasatch hingeline (e.g., DeCelles, 2004; DeCelles and Graham, 2015; Yonkee and Weil, 2015).

At the latitude of our study area (~39°N), the total shortening accommodated in the Sevier thrust belt is estimated at 220 km (DeCelles and Coogan, 2006). Deformation in the Sevier thrust belt initiated with displacement on the Canyon Range thrust between ca. 145–110 Ma (Fig. 14). The Canyon Range thrust carries an ~15-km-thick Neoproterozoic–Mesozoic section and accommodated as much as ~117 km of E-vergent displacement (Currie, 2002; DeCelles and Coogan, 2006). Based on subsurface geometric constraints, it is likely that this offset estimate is a maximum (e.g., DeCelles and Coogan, 2006), and the ca. 145 Ma estimate for the timing of initial slip on the Canyon Range thrust could also be a maximum (e.g., Yonkee and Weil, 2015). Initiation of motion on the Canyon Range thrust represented an ~300 km eastward jump in the Cordilleran thrust front, as estimated from the restored distance between the Luning-Fencemaker thrust belt in western Nevada and the trace of the Canyon Range thrust in west-central Utah on the restored cross section of Long (2019). This defines an accretion event that incorporated the upper crust of much of Nevada and western Utah.

Following emplacement of the Canyon Range thrust, deformation migrated foreland-ward to the Pavant thrust system, which carries the much thinner (≤~5 km) section of Paleozoic–Mesozoic rocks deposited east of the Wasatch hingeline (DeCelles et al., 1995; Currie, 2002). This consisted of displacement on the Pavant thrust between ca. 110–93 Ma, followed by duplexing in its footwall between ca. 93–88 Ma (DeCelles and Coogan, 2006) (Fig. 14). The duplexing coincided with the basal décollement

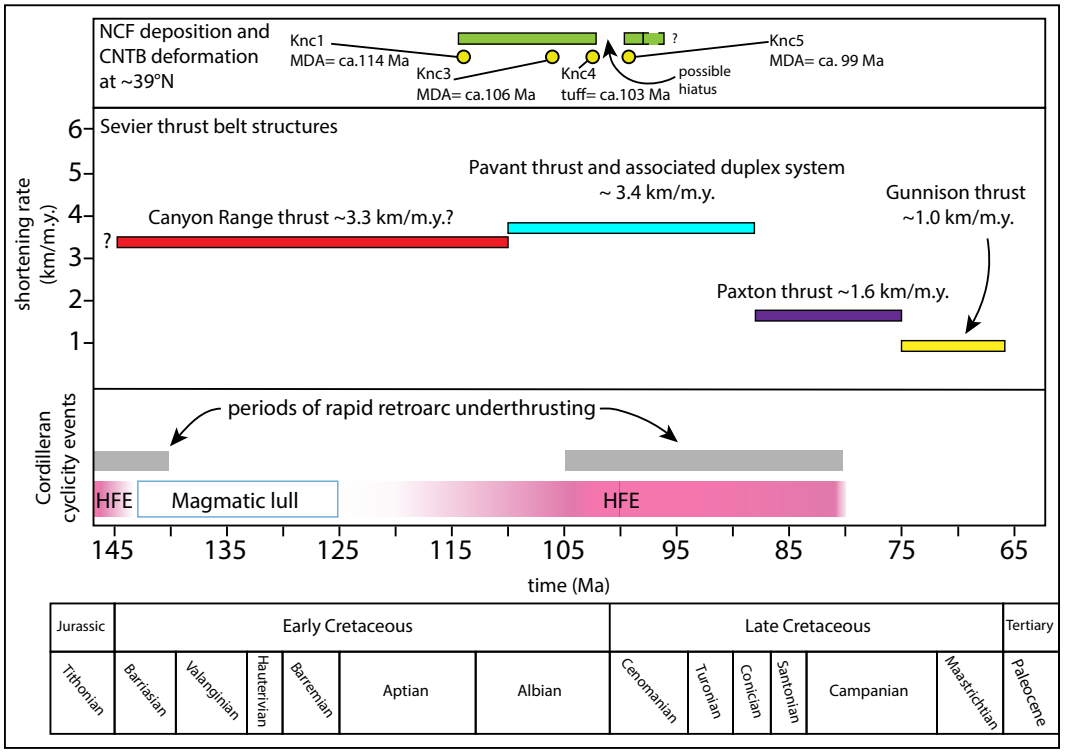

Figure 14. Chart showing timing and shortening rates of structural systems in the Sevier thrust belt at approximately the same latitude as our study in the Central Nevada thrust belt (CNTB) (calculated from DeCelles and Coogan, 2006, their figure 8). Timing constraints for Newark Canyon Formation (NCF) deposition and related CNTB deformation from our study are shown at the top. Abbreviations: NCF—Newark Canyon Formation; MDA—maximum depositional age; HFE—high flux event. Cordilleran cyclicity events are from DeCelles and Graham (2015). The timing of the magmatic lull is from Paterson and Ducea (2015).

climbing upward into a flat within weak Jurassic shale and evaporites (Currie, 2002; DeCelles and Coogan, 2006). The total shortening accommodated by the Pavant thrust and associated duplexing is estimated at ~74 km (DeCelles and Coogan, 2006). Following this, emplacement of the frontal Paxton and Gunnison thrust systems accommodated ~30 km of shortening between ca. 88 and ca. 66 Ma, primarily through duplexing and construction of a frontal triangle zone (Lawton et al., 1993; DeCelles et al., 1995).

Contractional deformation in the northern CNTB, as recorded by the deposition and folding of the NCF at ~39°N between ca. 103 Ma (and possibly as early as ca. 114 Ma) and at least ca. 99 Ma, records low-magnitude (~12–13 km) hinterland shortening during construction of the frontal Sevier thrust belt. Shortening in the CNTB overlapped temporally with emplacement of the Pavant thrust and associated duplex system (Fig. 14). Therefore, the CNTB preserves a record of partitioning of shortening between frontal and interior positions of the Cordilleran orogenic wedge. Because the CNTB was situated far to the west of the frontal, active portion of the Sevier thrust belt (~180 km, based on the distance between the NCF basin and the Pavant duplex on the restored cross section of Long, 2019), it is difficult to interpret this hinterland deformation in the context of critical taper dynamics. Instead, below we summarize several transitions that were taking place in the Cordilleran orogenic wedge during this time interval, in order to speculate on how the CNTB fits into this larger framework.

CNTB deformation immediately postdated a transition in structural style in the Sevier thrust belt, from emplacement of the thick Canyon Range thrust sheet to imbrication and duplexing of multiple thinner, frontal thrust sheets of the Pavant thrust and duplex system. This transition has been attributed to the thrust belt propagating eastward across the Wasatch hingeline, from the thick stratigraphy of the passive margin on the west to the thinner, less competent cratonic section on the east, eventually culminating in the basal décollement exploiting weak Jurassic shale and evaporites (e.g., DeCelles et al., 1995; Currie, 2002). In addition, CNTB deformation overlaps with the emplacement of the Pavant thrust sheet and associated duplex system between ca. 110–88 Ma, which records the fastest long-term shortening rates in the Sevier thrust belt at this latitude (DeCelles and Coogan, 2006) (Fig. 14).

A model for cyclical processes within the Cordillera recently put forth by DeCelles and Graham (2015) proposes a temporal link between high-flux

episodes in the magmatic arc and periods of rapid shortening and forward propagation in the retroarc thrust belt. In this model, high-flux magmatic events are interpreted as the result of rapid underthrusting of melt-fertile continental lower crust from the retroarc side, which is promoted by the foundering of a dense eclogitic root beneath the arc (DeCelles et al., 2009; DeCelles and Graham, 2015; Paterson and Ducea, 2015). NCF deposition and corresponding CNTB deformation at ~39°N were contemporary with a high-flux magmatic episode at ca. 115–80 Ma and the onset of renewed eastward propagation of the Sevier thrust belt (DeCelles and Graham, 2015, their figure 2). When viewed in the context of the cyclicity model, we speculate that CNTB deformation does not necessarily represent out-of-sequence deformation for building wedge taper, but instead may have represented synchronous partitioning of shortening between foreland (emplacement of the Pavant thrust and associated duplex system) and interior regions of the orogenic wedge (CNTB) in an effort to accommodate an overall increase in strain rates during renewed underthrusting.

In summary, deformation in the CNTB at our studied latitude corresponded temporally with a transition in structural style within the Sevier thrust belt, the interval of the highest shortening rates recorded in the Sevier thrust belt, a high-flux event in the magmatic arc, and an associated renewal of rapid underthrusting in the retroarc. We suggest that these factors worked together to promote partitioning of shortening between the frontal and interior portions of the orogenic wedge during the middle Cretaceous (ca. 115–90 Ma).

CONCLUSIONS

(1) In the southern Diamond Mountains, deposition of the basal member of the NCF began no earlier than ca. 114 Ma, middle members were being deposited by ca. 106–103 Ma, and the youngest member was deposited no earlier than ca. 99 Ma.

(2) Intraformational progressive unconformities, an angular unconformity between two members, and abrupt along- and across-strike thickness changes indicate that NCF deposition was coeval with growth of the east-vergent Strahlenberg anticline, a fault-propagation fold that we correlate with proximal CNTB deformation. This is corroborated by east-directed paleocurrents and clast compositions that define unroofing of upper Paleozoic sedimentary rocks, which we relate to the progressive erosion of a regional-scale CNTB anticline ~10 km to the west.

(3) CNTB deformation represents middle Cretaceous strain partitioning between frontal and interior components of the Cordilleran retroarc; this partitioning took place during a transition in the structural style in the Sevier thrust belt and during a time of high-flux magmatism and renewed retroarc shortening.

ACKNOWLEDGMENTS

This work was funded by National Science Foundation grant EAR-1524765 awarded to Long, Snell, and Bonde. We thank Kevin Rafferty for help and company while conducting field work. We also thank Da Wang and Charles Knaack for help with LA-ICPMS U-Pb analyses at the WSU Geochronology Laboratory.

REFERENCES CITED

Allmendinger, R.W., 1992, Fold and thrust tectonics of the western United States exclusive of the accreted terranes, *in* Burchfiel, B.C., et al., eds., The Cordilleran Orogen: Conterminous U.S.: Boulder, Colorado, Geological Society of America, Geology of North America, v. G-3, p. 583–608, https://doi.org/10.1130/DNAG-GNA-G3.583.

Anderson, R.B., Long, S.P., Horton, B.K., Thomson, S.N., Calle, A.Z., and Stockli, D.F., 2018, Orogenic wedge evolution of the central Andes, Bolivia (21°S): Implications for Cordilleran cyclicity: Tectonics, v. 37, p. 3577–3609, https://doi.org/10.1029/2018TC005132.

Armstrong, R.L., 1968, Sevier orogenic belt in Nevada and Utah: Geological Society of America Bulletin, v. 79, p. 429–458, https://doi.org/10.1130/0016-7606(1968)79[429:SOBINA]2.0.CO;2.

Atwater, T., 1970, Implications of plate tectonics for the Cenozoic evolution of North America: Geological Society of America Bulletin, v. 81, p. 3513–3536, https://doi.org/10.1130/0016-7606(1970)81[3513:IOPTFT]2.0.CO;2.

Best, M.G., Barr, D.L., Christiansen, E.H., Gromme, S., Deino, A.L., and Tingey, D.G., 2009, The Great Basin Altiplano during the middle Cenozoic ignimbrite flareup: Insights from volcanic rocks: International Geology Review, v. 51, p. 589–633, https://doi.org/10.1080/00206810902867690.

Bowring, S.A., and Schmitz, M.D., 2003, High-precision U-Pb zircon geochronology and the stratigraphic record: Reviews in Mineralogy and Geochemistry, v. 53, no. 1, p. 305–326.

Burchfiel, B.C., Cowan, D.S., and Davis, G.A., 1992, Tectonic overview of the Cordilleran orogen in the western United States, *in* Burchfiel, B.C., Lipman, P.W., and Zoback, M.L., eds., The Cordilleran Orogen: Conterminous U.S.: Boulder, Colorado, Geological Society of America, The Geology of North America, v. G-3, p. 407–480, https://doi.org/10.1130/DNAG-GNA-G3.407.

Carpenter, D.G., Carpenter, J.A., Dobbs, S.W., and Stuart, C.K., 1993, Regional structural synthesis of Eureka fold-and-thrust belt, east-central Nevada, *in* Gillespie, C.W., ed., Structural and Stratigraphic Relationships of Devonian Reservoir Rocks, East-Central Nevada: Reno, Nevada Petroleum Society, 1993 Field Conference Guidebook, p. 59–72.

Cassel, E.J., Breecker, D.O., Henry, C.D., Larson, T.E., and Stockli, D.F., 2014, Profile of a paleo-orogen: High topography across the present-day Basin and Range from 40 to 23 Ma: Geology, v. 42, p. 1007–1010, https://doi.org/10.1130/G35924.1.

Chang, Z., Vervoort, J.D., McClelland, W.C., and Knaack, C., 2006, U-Pb dating of zircon by LA-ICP-MS: Geochemistry, Geophysics, Geosystems, v. 7, Q05009, https://doi.org/10.1029/2005GC001100.

Colgan, J.P., and Henry, C.D., 2009, Rapid middle Miocene collapse of the Sevier orogenic plateau in north-central Nevada: International Geology Review, v. 51, p. 920–961, https://doi.org/10.1080/00206810903056731.

Coney, P.J., and Harms, T.J., 1984, Cordilleran metamorphic core complexes: Cenozoic extensional relics of Mesozoic compression: Geology, v. 12, p. 550–554, https://doi.org/10.1130/0091-7613(1984)12<550:CMCCCE>2.0.CO;2.

Coutts, D.S., Matthews, W.A., and Hubbard, S.M., 2019, Assessment of widely used methods to derive depositional ages from detrital zircon populations: Geoscience Frontiers, v. 10, p. 1421–1435, https://doi.org/10.1016/j.gsf.2018.11.002.

Currie, B.S., 2002, Structural configuration of the Early Cretaceous Cordilleran foreland-basin system and Sevier thrust belt, Utah and Colorado: The Journal of Geology, v. 110, p. 697–718, https://doi.org/10.1086/342626.

DeCelles, P.G., 1994, Late Cretaceous–Paleocene synorogenic sedimentation and kinematic history of the Sevier thrust belt, northeast Utah and southwest Wyoming: Geological Society of America Bulletin, v. 106, p. 32–56, https://doi.org/10.1130/0016-7606(1994)106<0032:LCPSSA>2.3.CO;2.

DeCelles, P.G., 2004, Late Jurassic to Eocene evolution of the Cordilleran thrust belt and foreland basin system, western U.S.A: American Journal of Science, v. 304, p. 105–168, https://doi.org/10.2475/ajs.304.2.105.

DeCelles, P.G., and Coogan, J.C., 2006, Regional structure and kinematic history of the Sevier fold-and-thrust belt, central Utah: Geological Society of America Bulletin, v. 118, p. 841–864, https://doi.org/10.1130/B25759.1.

DeCelles, P.G., and Currie, B.S., 1996, Long-term sediment accumulation in the Middle Jurassic–early Eocene Cordilleran retroarc foreland-basin system: Geology, v. 24, p. 591–594, https://doi.org/10.1130/0091-7613(1996)024<0591:LTSAIT>2.3.CO;2.

DeCelles, P.G., and Graham, S.A., 2015, Cyclical processes in the North American Cordilleran orogenic system: Geology, v. 43, p. 499–502, https://doi.org/10.1130/G36482.1.

DeCelles, P.G., Lawton, T.F., and Mitra, G., 1995, Thrust timing, growth of structural culminations, and synorogenic sedimentation in the type Sevier orogenic belt, western United

States: Geology, v. 23, p. 699–702, https://doi.org/10.1130/0091-7613(1995)023<0699:TTGOSC>2.3.CO;2.

DeCelles, P.G., Ducea, M.N., Kapp, P., and Zandt, G., 2009, Cyclicity in Cordilleran orogenic systems: Nature Geoscience, v. 2, p. 251–257, https://doi.org/10.1038/ngeo469.

Dickinson, W.R., 1974, Plate tectonics and sedimentation, *in* Dickinson, W.R., ed., Tectonics and Sedimentation: Society of Economic Paleontologists and Mineralogists (SEPM) Special Publication 22, p. 1–27, https://doi.org/10.2110/pec.74.22.0001.

Dickinson, W.R., 1988, Provenance and sediment dispersal in relation to paleotectonics and paleogeography of sedimentary basins, *in* Kleinspehn, K.L., and Paola, C., eds., New Perspectives in Basin Analysis: Berlin, Springer-Verlag, p. 3–25, https://doi.org/10.1007/978-1-4612-3788-4_1.

Dickinson, W.R., 2002, The Basin and Range province as a composite extensional domain: International Geology Review, v. 44, p. 1–38, https://doi.org/10.2747/0020-6814.44.1.1.

Dickinson, W.R., 2004, Evolution of the North American Cordillera: Annual Review of Earth and Planetary Sciences, v. 32, p. 13–45, https://doi.org/10.1146/annurev.earth.32.101802.120257.

Dickinson, W.R., 2006, Geotectonic evolution of the Great Basin: Geosphere, v. 2, p. 353–368, https://doi.org/10.1130/GES00054.1.

Dickinson, W.R., and Gehrels, G.E., 2009, Use of U-Pb ages of detrital zircons to infer maximum depositional ages of strata: A test against a Colorado Plateau Mesozoic database: Earth and Planetary Science Letters, v. 288, p. 115–125, https://doi.org/10.1016/j.epsl.2009.09.013.

Druschke, P., Hanson, A.D., Wells, M.L., Gehrels, G.E., and Stockli, D., 2011, Paleogeographic isolation of the Cretaceous to Eocene Sevier hinterland, east-central Nevada: Insights from U-Pb and (U-Th)/He detrital zircon ages of hinterland strata: Geological Society of America Bulletin, v. 123, p. 1141–1160, https://doi.org/10.1130/B30029.1.

Fouch, T.D., Hanley, J.M., and Forester, R.M., 1979, Preliminary correlation of Cretaceous and Paleogene lacustrine and related nonmarine sedimentary and volcanic rocks in parts of the Great Basin of Nevada and Utah, *in* Newman, G.W., and Goode, H.D., eds., Basin and Range Symposium and Great Basin Field Conference: Rocky Mountain Association of Petroleum Geologists and Utah Geological Association, p. 305–312.

French, D.E., 1993, Thrust faults in the southern Diamond Mountains, Eureka and White Pine counties, Nevada, *in* Gillespie, C.W., ed., Structural and Stratigraphic Relationships of Devonian Reservoir Rocks, East-Central Nevada: Nevada Petroleum Society 1993 Field Conference Guidebook NPS 07, p. 105–114.

Gans, P.B., and Miller, E.L., 1983, Style of mid-Tertiary extension in east-central Nevada, *in* Gurgel, K.D., ed., Geologic Excursions in the Overthrust Belt and Metamorphic Core Complexes of the Intermountain Region: Utah Geological and Mineral Survey Special Studies Volume 59, p. 107–160.

Gehrels, G.E., Valencia, V., and Ruiz, J., 2008, Enhanced precision, accuracy, efficiency, and spatial resolution of U-Pb ages by laser ablation–multicollector–inductively coupled plasma–mass spectrometry: Geochemistry, Geophysics, Geosystems, v. 9, Q03017, https://doi.org/10.1029/2007GC001805.

Greene, D.C., 2014, The Confusion Range, west-central Utah: Fold-thrust deformation and a western Utah thrust belt in the Sevier hinterland: Geosphere, v. 10, p. 148–169, https://doi.org/10.1130/GES00972.1.

Hague, A., 1892, Geology of the Eureka district, Nevada: U.S. Geological Survey Monograph 20, 419 p., 13 sheets.

Horton, B.K., Constenius, K.N., and DeCelles, P.G., 2004, Tectonic control on coarse-grained foreland-basin sequences: An example from the Cordilleran foreland basin, Utah: Geology, v. 32, p. 637–640, https://doi.org/10.1130/G20407.1.

Humphreys, E.D., 1995, Post-Laramide removal of the Farallon slab, western United States: Geology, v. 23, p. 987–990, https://doi.org/10.1130/0091-7613(1995)023<0987:PLROTF>2.3.CO;2.

Larsen, E.R., and Riva, J.F., 1963, Preliminary geologic map of the Diamond Springs quadrangle, Nevada: Nevada Bureau of Mines and Geology Map #20, scale 1: 62,500.

Lawton, T.F., 1983, Late Cretaceous fluvial systems and the age of foreland uplifts in central Utah, *in* Lowell, J. D., ed., Rocky Mountain Foreland Basins and Uplifts: Denver, Colorado, Rocky Mountain Association of Geologists, p. 181–199.

Lawton, T.F., Talling, P.J., Hobbs, R.S., Trexler, J.H., Jr., Weiss, M.P., and Burbank, D.W., 1993, Structure and stratigraphy of Upper Cretaceous and Paleogene strata (North Horn Formation), eastern San Pitch Mountains, Utah—Sedimentation at the front of the Sevier orogenic belt: U.S. Geological Survey Bulletin 1787, p. 111–133.

Lawton, T.F., Sprinkel, D., DeCelles, P.G., Mitra, G., and Sussman, A.J., 1997, Thrusting and synorogenic sedimentation in the central Utah Sevier thrust belt and foreland basin: Brigham Young University Geology Studies, v. 42, part 2, p. 33–67.

Lee, J., Blackburn, T., and Johnston, S., 2017, Timing of mid-crustal ductile extension in the northern Snake Range metamorphic core complex, Nevada: Evidence from U/Pb zircon ages: Geosphere, v. 13, no. 2, p. 439–459, https://doi.org/10.1130/GES01429.1.

Long, S.P., 2012, Magnitudes and spatial patterns of erosional exhumation in the Sevier hinterland, eastern Nevada and western Utah, USA: Insights from a Paleogene paleogeologic map: Geosphere, v. 8, p. 881–901, https://doi.org/10.1130/GES00783.1.

Long, S.P., 2015, An upper-crustal fold province in the hinterland of the Sevier orogenic belt, eastern Nevada, U.S.A.: A Cordilleran Valley and Ridge in the Basin and Range: Geosphere, v. 11, p. 404–424, https://doi.org/10.1130/GES01102.1.

Long, S.P., 2019, Geometry and magnitude of extension in the Basin and Range Province (39°N), California, Nevada, and Utah, USA: Constraints from a province-scale cross section: Geological Society of America Bulletin, v. 131, p. 99–119, https://doi.org/10.1130/B31974.1.

Long, S.P., Henry, C.D., Muntean, J.L., Edmondo, G.P., and Cassel, E.J., 2014, Early Cretaceous construction of a structural culmination, Eureka, Nevada, U.S.A.: Implications for out-of-sequence deformation in the Sevier hinterland: Geosphere, v. 10, p. 564–584, https://doi.org/10.1130/GES00997.1.

Long, S.P., Heizler, M.T., Thomson, S.N., Reiners, P.W., and Fryxell, J.E., 2019, Rapid Oligocene to early Miocene extension along the Grant Range detachment system, eastern Nevada, USA: Insights from multi-part cooling histories of footwall rocks: Tectonics, v. 37, p. 4752–4779, https://doi.org/10.1029/2018TC005073.

Ludwig, K.R., 2008, User's Manual for Isoplot 3.6: Geochronological Toolkit for Microsoft: Berkeley Geochronology Center Special Publication 4, 78 p.

MacNeil, F.S., 1939, Fresh-water invertebrates and land plants of Cretaceous age from Eureka, Nevada: Journal of Paleontology, v. 13, p. 355–360.

McQuarrie, N., 2002, The kinematic history of the central Andean fold-thrust belt, Bolivia: Implications for building a high plateau: Geological Society of America Bulletin, v. 114, no. 8, p. 950–963, https://doi.org/10.1130/0016-7606(2002)114<0950:TKHOTC>2.0.CO;2.

Morley, C.K., 1988, Out-of-Sequence Thrusts: Tectonics, v. 7, no. 3, p. 539–561, https://doi.org/10.1029/TC007i003p00539.

Nolan, T.B., 1962, The Eureka mining district, Nevada: U.S. Geological Survey Professional Paper 406, 78 p.

Nolan, T.B., Merriam, C.W., and Williams, J.S., 1956, The Stratigraphic Section in the Vicinity of Eureka, Nevada: U.S. Geological Survey Professional Paper 276, 77 p., https://doi.org/10.3133/pp276.

Nolan, T.B., Merriam, C.W., and Brew, D.A., 1971, Geologic Map of the Eureka Quadrangle, Eureka and White Pine Counties, Nevada: U.S. Geological Survey Miscellaneous Investigations Series Map I-612, scale 1:31,680, 8 p., 2 plates.

Nolan, T.B., Merriam, C.W., and Blake, M.C., Jr., 1974, Geologic Map of the Pinto Summit Quadrangle, Eureka and White Pine Counties, Nevada: U.S. Geological Survey Miscellaneous Investigations Series Map I-793, scale 1: 31,680, 14 p., 2 plates.

Oldow, J.S., 1984, Evolution of a late Mesozoic back-arc fold and thrust belt, northwestern Great Basin, U.S.A: Tectonophysics, v. 102, p. 245–274, https://doi.org/10.1016/0040-1951(84)90016-7.

Paterson, S.R., and Ducea, M.N., 2015, Arc magmatic tempos: Gathering the evidence: Elements, v. 11, p. 91–98, https://doi.org/10.2113/gselements.11.2.91.

Poole, F.G., Stewart, J.H., Palmer, A.R., Sandberg, C.A., Madrid, R.J., Ross, R.J., Jr., Hintze, L.F., Miller, M.M., and Wricke, C.T., 1992, Latest Precambrian to latest Devonian time: Development of a continental margin, *in* Burchfiel, B.C., Lipman, P.W., and Zoback, M.L., eds., The Cordilleran Orogen: Conterminous U.S.: Boulder, Colorado, Geological Society of America, The Geology of North America, v. G-3, p. 9–56, https://doi.org/10.1130/DNAG-GNA-G3.9.

Riba, O., 1976, Syn-tectonic unconformities in the Alto Cardener, Spanish Pyrenees: Genetic interpretation: Sedimentary Geology, v. 15, no. 3, p. 213–233.

Smith, M.E., Carroll, A.R., Jicha, B.J., Cassel, E.J., and Scott, J.J., 2014, Paleogeographic record of Eocene Farallon slab rollback beneath western North America: Geology, v. 42, p. 1039–1042, https://doi.org/10.1130/G36025.1.

Snell, K.E., Koch, P.L., Druschke, P., Foreman, B.Z., and Eiler, J.M., 2014, High elevation of the 'Nevadaplano' during the Late Cretaceous: Earth and Planetary Science Letters, v. 386, p. 52–63, https://doi.org/10.1016/j.epsl.2013.10.046.

Speed, R.C., and Sleep, N., 1982, Antler orogeny and foreland basin: A model: Geological Society of America Bulletin, v. 93, p. 815–828, https://doi.org/10.1130/0016-7606(1982)93<815:AOAFBA>2.0.CO;2.

Stewart, J.H., 1980, Geology of Nevada: A discussion to accompany the Geologic Map of Nevada: Nevada Bureau of Mines and Geology Special Publication 4, 136 p.

Stewart, J.H., and Poole, F.G., 1974, Lower Paleozoic and uppermost Precambrian Cordilleran miogeocline, Great Basin, western United States, *in* Dickinson, W.R., ed., Tectonics and

Sedimentation: SEPM (Society of Economic Paleontologists and Mineralogists) Special Publication 22, p. 28–57, https://doi.org/10.2110/pec.74.22.0028.

Suppe, J., and Medwedeff, D.A., 1990, Geometry and kinematics of fault-propagation folding: Eclogae Geologicae Helvetiae, v. 83, p. 409–454.

Taylor, W.J., Bartley, J.M., Martin, M.W., Geissman, J.W., Walker, J.D., Armstrong, P.A., and Fryxell, J.E., 2000, Relations between hinterland and foreland shortening: Sevier orogeny, central North American Cordillera: Tectonics, v. 19, p. 1124–1143, https://doi.org/10.1029/1999TC001141.

Vandervoort, D.S., 1987, Sedimentology, Provenance, and Tectonic Implications of the Cretaceous Newark Canyon Formation, East-Central Nevada [M.S. thesis]: Bozeman, Montana State University, 145 p.

Vandervoort, D.S., and Schmitt, J.G., 1990, Cretaceous to early Tertiary paleogeography in the hinterland of the Sevier thrust belt, east-central Nevada: Geology, v. 18, p. 567–570, https://doi.org/10.1130/0091-7613(1990)018<0567:CTETPI>2.3.CO;2.

Villien, A., and Kligfield, R.M., 1986, Thrusting and synorogenic sedimentation in central Utah, *in* Peterson, J.A., ed., Paleotectonics and Sedimentation in the Rocky Mountain Region, United States: American Association of Petroleum Geologists Memoir 41, p. 281–308, https://doi.org/10.1306/M41456C13.

Wells, M.L., Hoisch, T.D., Cruz-Uribe, A.M., and Vervoort, J.D., 2012, Geodynamics of synconvergent extension and tectonic mode switching: Constraints from the Sevier-Laramide orogen: Tectonics, v. 31, TC1002.

Wyld, S.J., 2002, Structural evolution of a Mesozoic backarc fold-and-thrust belt in the U.S. Cordillera: New evidence from northern Nevada: Geological Society of America Bulletin, v. 114, p. 1452–1468, https://doi.org/10.1130/0016-7606(2002)114<1452:SEOAMB>2.0.CO;2.

Yonkee, W.A., and Weil, A.B., 2015, Tectonic evolution of the Sevier and Laramide belts within the North American Cordillera orogenic system: Earth-Science Reviews, v. 150, p. 531–593, https://doi.org/10.1016/j.earscirev.2015.08.001.

Yonkee, W.A., DeCelles, P.G., and Coogan, J.C., 1997, Kinematics and synorogenic sedimentation of the eastern frontal part of the Sevier orogenic wedge, northern Utah, *in* Link, P.K., and Kowallis, B.J., eds., Proterozoic to Recent Stratigraphy, Tectonics, and Volcanology, Utah, Nevada, Southern Idaho and Central Mexico: Brigham Young University Geology Studies, v. 42, part 1, p. 355–380.